Journal of Hazardous Materials 423 (2022) 126996

Contents lists available at ScienceDirect

Journal of Hazardous Materials

journal homepage: www.elsevier.com/locate/jhazmat

A review on self-modification of zirconium dioxide nanocatalysts with enhanced visible-light-driven photodegradation of organic pollutants

N.S. Hassan [a], A.A. Jalil [a,b,*]

[a] School of Chemical and Energy Engineering, Faculty of Engineering, Universiti Teknologi Malaysia, 81310 UTM Johor Bahru, Johor, Malaysia
[b] Centre of Hydrogen Energy, Institute of Future Energy, 81310 UTM Johor Bahru, Johor, Malaysia

ARTICLE INFO

Editor: Dr. Rinklebe Jörg

Keywords:
Zirconium dioxide
Nanocatalyst
Self-modification
Photodegradation
Organic pollutants

ABSTRACT

Over the past few years, photocatalysis is one of the most promising approaches for removing organic pollutants. Zirconium dioxide (ZrO_2) has been shown to be effective in the photodegradation of organic pollutants. However, low photoresponse and fast electron-hole recombination of ZrO_2 affected the efficiency of catalytic performance. Modifying the photocatalyst itself (self-modification) is a prominent way to enhance the photoactivity of ZrO_2. Moreover, as ZrO_2-like photocatalysts have a large bandgap, improving the spectral response via self-modification could extend the visible light region and reduce the chance of recombination. Here, we review the self-modification of ZrO_2 for enhanced the degradation of organic pollutants. The approaches of the ZrO_2 self-modification, including the type of synthetic route and synthesis parameter variation, are discussed in the review. This will be followed by a brief section on the effect of ZrO_2 self-modification in terms of morphology, crystal structure, and surface defects for enhanced photodegradation efficiency. It also covers the discussion on the photocatalytic mechanism of ZrO_2 self-modification. Finally, some challenges with ZrO_2 catalysts are also discussed to promote new ideas to improve photocatalytic performance.

1. Introduction

The toxicity and adverse effects of chemical pollutants released by the agricultural sectors and industries significantly impact the surroundings, particularly human health and aquatic life (Azami et al., 2021; Hassan et al., 2021a; Mahy et al., 2019). The majority of aromatic and organic substances are difficult to break down and can lead to catastrophic chronic illnesses (Siwińska-Ciesielczyk et al., 2020; Aziz et al., 2018). Accordingly, various treatment techniques have been employed, such as coagulation, adsorption, electrochemical degradation, and ion exchange, to mitigate the environmental impact of hazardous and resistant pollutants (Hassan et al., 2020; López et al., 2019). However, these processes have several drawbacks, including the high amount of sludge and secondary products formed, time-consuming, and costly (Fauzi et al., 2020). Consequently, research initiatives aimed at developing ways for environmentally friendly and green treatments are critical. An advanced oxidation process (AOP), which employs heterogeneous semiconductors to remove pollutants without causing secondary pollution, appears to be a promising approach (Aziz et al., 2021, 2020).

In the past two decades, titanium dioxide (TiO_2) is frequently utilized as a photocatalyst to degrade organic compounds (Gnanasekaran et al., 2021; Hitam et al., 2018; Mustapha et al., 2017). However, TiO_2 tends to aggregate and is uneconomical for large-scale production (Rahman et al., 2017). Zirconium dioxide (ZrO_2) has gained much interest as a photocatalyst to replace the use of TiO_2 since it has similar physicochemical properties to TiO_2, including higher thermal stability (Melchor-Lagar et al., 2020; Hassan et al., 2019; Suresh et al., 2014; Sapawe et al., 2012). Undoubtedly, ZrO_2 has a low surface area (23 m^2/g) and only can be applied under ultra-violet (UV) light (wavelength, $\lambda < 388$ nm) due to its wide bandgap (E_g, 5.0 eV), which means limited usage of incoming solar energy on the earth surface (~4%), thus hindered its photocatalytic efficiency (Teeparthi et al., 2018; Jalil et al., 2015).

Two ways widely used to broaden the spectral response of photocatalysts are extra-modification and self-modification (Nasir et al., 2020). Self-modification refers to the process of altering a photocatalyst's structure and surface, whereas extra-modification refers to the incorporation of additional material (Li et al., 2016). A quick search of the available literature reveals that there are many different types of original research works and reviews over the extra-modification of

* Corresponding author at: School of Chemical and Energy Engineering, Faculty of Engineering, Universiti Teknologi Malaysia, 81310 UTM Johor Bahru, Johor, Malaysia.
E-mail address: aishahaj@utm.my (A.A. Jalil).

https://doi.org/10.1016/j.jhazmat.2021.126996
Received 9 June 2021; Received in revised form 2 August 2021; Accepted 19 August 2021
Available online 21 August 2021
0304-3894/

photocatalyst to improve catalytic activity. In addition, extra-modification of a ZrO_2 photocatalyst by incorporating additional materials is an effective way of modification (Fang et al., 2017). However, light blockage on the catalyst's surface may occur due to additional materials, and this effect should be considered. Furthermore, these materials served as recombination centers for produced holes (h^+) and electrons (e^-), which is detrimental to the photocatalytic process's efficiency (Lin et al., 2017).

Because ZrO_2-like photocatalysts have a large E_g, improving the spectral response via self-modification could extend the visible light region and reduce the odds of recombination. To the best of our knowledge, no comprehensive review has been published yet on the self-modification of any photocatalyst, especially on the development of ZrO_2 structure to enhance the degradation of organic pollutants. Therefore, we attempt to explore self-modifications on ZrO_2 photocatalysts in this review. The approaches, effect, and photocatalytic mechanism of ZrO_2 self-modification are discussed in this review. This review is intended to aid in understanding the current state of ZrO_2 photocatalyst development and stimulate self-modifications for improving photocatalytic activities.

2. Photocatalysis

Photocatalysis is defined as a photoreaction acceleration process by the action of a catalyst under light irradiation. The earlier IUPAC document describes it as a reaction medium, which involves light absorption (Fagan et al., 2016). The expression "photocatalysis" is derived from two Greek words: "photo" (phos: light) and "catalysis" (katalyo: break apart, decompose). A photocatalyst is an active substance that alters the rate of a chemical process without causing harm to the catalyst. In the 1970 s, after discovering photolysis of water-assisted by TiO_2 electrode by Fujishima and Honda (1972), the concept of photocatalysis has become a vital and unavoidable technology. Nowadays, photocatalytic technology is applied in the effective removal of toxic substances and pathogens from water and air medium (Suresh et al., 2021), the production of hydrogen gas by water splitting reaction, production of pharmaceutically important organic compounds, treatment of cancer cells, and self-cleaning coatings. This technology mainly uses solar energy, a renewable energy resource, and reduces pollution concerns significantly.

Generally, there are two types of photocatalysts: homogeneous and heterogeneous photocatalysts. A homogeneous photocatalyst consists of Fenton's reagent, light-assisted Fenton's oxidation, ozonation, and H_2O_2/UV treatment (Sathishkumar et al., 2015; Dutta et al., 2015; Xavier et al., 2015; Yaghmaeian et al., 2014). This system is called a single-phase system due to the same phase of the catalyst and reactants. Meanwhile, heterogeneous photocatalysis is semiconductor-mediated, involving different phases of catalyst and reactants (Xavier et al., 2015). The heterogeneous photocatalysis exhibits extra advantages on stability in terms of temperature, recyclability, and the ability to achieve the complete removal of organic pollutants.

AOP is a part of the chemical treatment and heterogeneous photocatalysis, which has become an emerging technology in purifying wastewater due to its ability to solve many problems resulting from other conventional techniques (Gnanasekaran et al., 2021). AOP deals with the generation and use of reactive free radicals to oxidize and convert complex dissolved effluents into more specific and nontoxic products (Rajendran et al., 2021; Dhiman et al., 2017). The oxidation process undergoes an e^- transfer, which results in the chemical transformation of species known as radicals (Suresh et al., 2021). The generated free radical is reactive due to the presence of unpaired e^-, which makes it unstable. AOPs usually involve redox reactions in which both reduction and oxidation coincided (Zhang et al., 2014).

The strength of the oxidant is significant and is called oxidation potential. Hydroxyl radical (·OH), fluorine, ozone, and chlorine are common oxidants used, and their oxidation states are 2.85, 2.70, 2.07, and 1.49 eV, respectively (Lutterbeck et al., 2015). Among them,·OH radical has the highest oxidation potential than other oxidants (Pourakbar et al., 2016). Chemical oxidation does not produce a large amount of chemical or biological sludge, and a complete breakdown of organic contaminants can be achieved, giving AOP significant advantages over conventional treatments (Oturan and Aaron, 2014). However, the main problems of AOP are the high cost of reagents and usage of UV light as their energy source (Rodriguez-Chueca et al., 2016). A typical AOP pathway that involves UV/H_2O_2 comprises four steps. The steps are·OH radical initiation (Eq. (1)), propagation (Eqs. (2–3)), termination (Eqs. (4–6)), and decomposition (Eq. (7)) (Liu et al., 2015).

Initiation

$$H_2O_2 + hv \rightarrow 2^{\bullet}OH \quad (1)$$

Propagation

$$H_2O_2 + {}^{\bullet}OH \rightarrow HO_2{}^{\bullet} + H_2O \quad (2)$$

$$H_2O_2 + HO_2{}^{\bullet} \rightarrow {}^{\bullet}OH + H_2O + O_2 \quad (3)$$

Termination

$$2^{\bullet}OH \rightarrow H_2O_2 \quad (4)$$

$$2HO_2{}^{\bullet} \rightarrow H_2O_2 + O_2 \quad (5)$$

$${}^{\bullet}OH + HO_2 \rightarrow {}^{\bullet}H_2O + O_2 \quad (6)$$

Decomposition

$$X + {}^{\bullet}OH \rightarrow X_{product} + H_2O + CO_2 \quad (7)$$

The absorption of photons initiates the reaction pathways in the heterogeneous photocatalysis process. The energy of absorbed photons, *hv*, should be greater or equal to the energy of the E_g. Moreover, the activated catalyst excites the e^- to the conduction band (CB) from the valence band (VB) and leaves h^+ at the VB. Hence, it promotes the production of·OH to attack most of the organic structure to be degraded into non-hazardous products. The general photocatalytic reaction is illustrated in Fig. 1, while its available mechanism is summarized in Table 1 (Jaafar et al., 2015).

Reduction and oxidation take place at the photo-excited surface of the photocatalyst. Recombination between e^- and h^+ can either occur for the use of redox reaction. The e^- and h^+ that do not recombine are transferred to the surface of redox reaction and undergo reduction process and oxidation process to form superoxide ion (·$O_2{}^-$) and·OH, respectively. The OH^- then leads to the production of strong oxidizing·OH radicals. Meanwhile, the negative e^- react with the oxygen

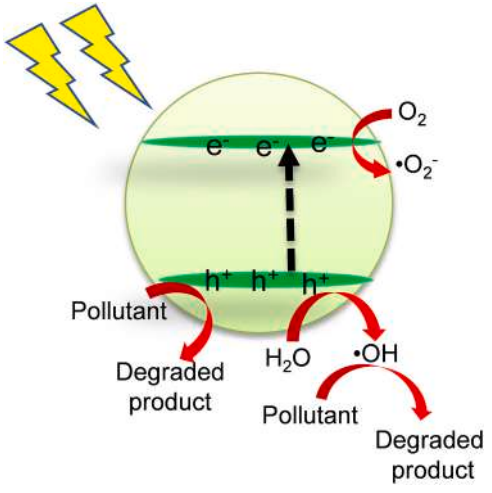

Fig. 1. General catalytic reaction under light irradiation.

Table 1
General mechanism of the photocatalytic reaction on semiconductor.

Process	Reaction Step
Photo-excited semiconductor(SC) generates electron–hole pairs	$SC \rightarrow^{hv} e^- + h^+$
To generated holes, h^+ migrate to catalyst surface and react with water molecules adsorbed on the catalyst surface H_2O_{ad}	$SC\ (h^+) + H_2O_{ad} \rightarrow SC + {}^{\cdot}OH + h^+$
Photogenerated electrons, e^- migrate to catalyst surface and molecular oxygen acts as an acceptor species in the electron-transfer reaction	$SC\ (e^-) + O_2 \rightarrow SC + O_2^{\bullet-}$
Reactions of superoxide anions, $\cdot O_2^-$	$O_2^{\bullet-} + H^+ \rightarrow HO_2^{\cdot}$ $O_2^{\bullet-} + 3\ HO_2^{\cdot} \rightarrow {}^{\cdot}OH + 3\ O_2 + H_2O + e^-$ $2\ HO_2^{\cdot} \rightarrow O_2 + H_2O_2$
Photoconversion of hydrogen peroxide to give more $HO^{\bullet}$ free-radical groups	$H_2O_2 + SC\ (e^-) \rightarrow SC + HO^- + {}^{\cdot}OH$
Oxidization of organic adsorbed pollutants (S_{ad}) by $HO^{\bullet}$ onto the surface of the SC	$HO_2^{\cdot} + S_{ad} \rightarrow$ Intermediates
Overall reaction	Organic pollutant$^{SC/hv} \rightarrow$ Intermediates $\rightarrow CO_2 + H_2O$

(O) molecule to form a $\cdot O_2^-$. This $\cdot O_2^-$ also produces ·OH radicals via the formation of $HO_2^{\bullet}$ radicals and H_2O_2 (Saravanan et al., 2013). The radicals formed from the reaction are used to degrade the organic pollutant.

Generally, TiO_2 is a commonly used heterogeneous photocatalyst due to its ability to oxidation of wide varieties of pollutants, inertness, high photocatalytic activity, low cost for large-scale production, greater mobility of electrons, and strong emission character (Suresh et al., 2021). Besides, their application in wastewater treatment is limited due to the less stability in water during photodegradation due to the different pH of the medium and dissolved oxygen content. These reasons lead researchers to perform modifications in TiO_2 or to find alternative photocatalytic materials. Recently, visible-light-driven photocatalysts are attracted worldwide; this is because of sunlight which comprises 46% of visible light and only 5% of ultraviolet light of the total solar energy. In this context, ZrO_2 as a visible light active material has gained attraction by scientists since the self-modifications improved the spectral response.

3. Zirconium dioxide (ZrO_2) as photocatalyst

Zirconium dioxide or zirconia (ZrO_2) is a white crystalline oxide semiconductor. The stable monoclinic (*m*-ZrO_2; < 1170 °C), metastable tetragonal (*t*-ZrO_2; >1170 <2370 °C), and cubic (*c*-ZrO_2; > 2370 °C) phases of ZrO_2 occur at different temperatures (Kumar and Ojha, 2015). Generally, ZrO_2 is a p-type semiconductor that exhibited acidic and basic characteristics (Aziz et al., 2021; Hassan et al., 2018b; Teeparthi et al., 2018). The high negative value of CB potential and wide E_g of ZrO_2 could generate interaction with active sites due to the O holes as a catalyst carrier. In addition, those properties permit its usage as a photocatalyst in heterogeneous reactions, especially photodegradation of organic pollutants.

As tabulated in Table 2, ZrO_2 has been used as a photocatalyst for dyes and antibiotics degradation. Dyes are sided products from various manufacturing industries and are considered dangerous organic pollutants to the environment. Once these organics enter the water, they become more stable and more difficult to biodegrade, owing to their complex chemical structures. Thus, these issues in treating dye effluents from the textile industry have persisted over the last decade. For example, Moafi et al. (2010) stated that ZrO_2 shows a better performance in degrading eosin Y about 70%. Sultana et al. (2015) also synthesized the ZrO_2 for degradation of Acid Blue 25 (65%), and the ZrO_2 also showed remarkable antibacterial activity against two gram-negative (*Pseudomonas aeruginosa, Escherichia coli*) and two gram-positive (*Staphylococcus aureus, Bacillus subtilis*) strain. The ZrO_2 nanostructures also were used to degrade Eriochrome Black T and Rhodamine B about 72% and 86.2%, respectively (Zinatloo-Ajabshir et al., 2016; Wu et al., 2016).

Methylene blue (MB) is one of the common dyes widely used in the textile industry. The demand for textiles was increased day by day, which caused the environmental hazard since dyes provide bright and lasting color to other substances. The discharge of these highly colored wastes is aesthetically unpleasant and hinders light penetration, hence upsetting biological processes in the receiving water body. Thus, Jalil et al. (2015) synthesized *t*-ZrO_2, and this catalyst facilitated good photoactivity towards MB degradation (83.6%) under UV light in a batch reactor compared with commercial ZrO_2 (58.7%) and Degussa P25 TiO_2 (64.5%).. The excellent stability after five cycling runs and good mineralization of MB demonstrate the potential use of *t*-ZrO_2 in dye wastewater treatment. The catalyst stability is of great concern for wastewater treatment to reduce the operational cost (Teeparthi et al., 2018). A similar stability trend was also observed when ferromagnetic ZrO_2 nanostructures were tested on the degradation of MB under UV radiation for three cycles (Kumar et al., 2015).

Nawale et al. (2012) also synthesized ZrO_2 for MB degradation under UV radiation. As inferred from the photoabsorption measurements, different defect states and their concentration were responsible for the enhanced photocatalytic activity of the as-synthesized samples. These defect states are present due to the oxygen vacancy (OV) generated from the thermal plasma route. Stojadinović et al. (2015) also used the plasma electrolytic oxidation (PEO) method for the preparation of ZrO_2 films and applied the catalyst for the photodegradation of methyl orange (MO). However, the poor activity in MO degradation was attributed to the less crystalline structure of ZrO_2 and lower OV sites within thicker layers. The higher crystallinity of ZrO_2 improved the efficiency in MO

Table 2
Degradation of various pollutants using ZrO_2 as photocatalyst.

Reaction parameter			Lamp, Power (W)	Band gap (eV)	Degradation (%), Time (min)	Pollutant	References
pH	W (g L^{-1})	[P] (mg L^{-1})					
n.a	n.a	10	n.a	4.50	70.0, 360	Eosin Y	Moafi et al. (2010)
n.a	0.14	10	Kr, 400	3.06	100, 40	Methylene Blue	Nawale et al. (2012)
n.a	n.a	8.0	Solar, 300	4.30	25.0480	Methyl Orange	Stojadinovic et al., 2015
n.a	n.a	10	n.a	4.80	35.0, 60	Methylene Blue	Kumar and Ojha (2015)
9	0.30	20	UV	n.a	65.0, 75	Acid Blue 25	Sultana et al. (2015)
11	1.0	10	UV, 32	2.89	83.6, 240	Methylene Blue	Jalil et al. (2015)
n.a	n.a	n.a	n.a	n.a	85.0, 60	Methyl Orange	Majedi et al. (2016)
n.a	0.040	n.a	n.a	3.40	72.0, 120	Eriochrome Black T	Zinatloo-Ajabshir et al. (2016)
n.a	0.10	10	Hg, 120	3.30	86.2, 120	Rhodamine B	Wu et al. (2016)
n.a	0.50	30	Xe, 500	3.71	76.0, 300	Methylene Blue	Teeparthi et al. (2018)
n.a	1.0	40	Xe, 300	4.89	80.4, 150	Tetracycline hydrochloride	Zhang et al. (2018)
7	1.5	10	Hg, 250	4.90	91.0, 240	Methyl Orange	Shinde et al. (2018)
3	1.5	20	300	n.a	95.3, 90	Rifampin	Khataee et al. (2018)

W= Catalyst Dosage, [P]= Concentration of Pollutant, n.a=not available

degradation, as reported by Majedi and co-workers (Majedi et al., 2016). Similarly, Shinde et al. (2018) reported that the synthesized ZrO_2 NPs are crystalline in nature and exhibited higher performance in degrading the MO. Thus, it can be concluded that the catalyst's crystallinity could enhance the catalytic activity and subsequently contribute to the high potential for water decontamination.

Instead of dyes, lately, ZrO_2 has been found to degrade antibiotics, which are the most prosperous pharmaceuticals used to treat different infections. These compounds could have adverse effects on human health that are tough to anticipate. Zhang et al., (2018) stated that the OV-rich ZrO_2 exhibited excellent performance (80.4%) in degrading tetracycline hydrochloride (TCH). The better adsorption affinity and higher OV are beneficial for enhanced photocatalytic reaction. The former properties are also dependent on the surface acidity of a photocatalyst. In this study, the adsorption affinity can be related to weak acid sites rather than strong acid sites. Khataee et al. (2018) also synthesized ZrO_2 nanoparticles (NPs) for photocatalytic degradation of rifampin (RIF). These antibacterial prevent bacterial growth by interfering with bacterial ribonucleic acid synthesis. The ZrO_2 catalyst with a higher surface area had great photocatalytic activity. In addition, the surface of ZrO_2 catalysts was positively charged under acidic solution, which attractively bonded to anionic RIF, indicating that RIF molecules were present at higher concentrations around the surface of the catalyst, and they could be easily subjected to the reactive radicals. Thus, it can be concluded that surface adsorption affinity is a crucial factor for enhancing degradation performance.

In conclusion, the ZrO_2 is the widely used photocatalyst to degrade organic pollutants, particularly dyes and pharmaceutical compounds. The exceptional properties of the ZrO_2 in nanostructures, such as high crystallinity, surface adsorption affinity, and OV, contribute to the high potential for water decontamination.

4. Approaches of ZrO_2 self-modification

Currently, low photoresponse and fast recombination of photogenerated e^--h^+ pairs of ZrO_2 catalyst affected the efficiency of catalytic performance. To address this problem, modifying the photocatalyst or self-modification is an efficient technique for enhancing catalytic performance. Because increasing the spectral response via self-modification reduces the probabilities of recombination and extends the visible light region, it's a good technique for ZrO_2-like photocatalysts, which have a wide E_g. In addition, materials or photocatalysts in nanoscale also enhanced the catalytic performance. For this purpose, the type of synthetic route and synthesis parameter variation for preparation of ZrO_2 nanomaterials could be used as an approach for ZrO_2 self-modification, which have been explored in this section (Fig. 2).

4.1. Type of synthetic route

Over the last decade, ZrO_2 is considered a photocatalyst due to its high negative value of the CB potential and has wide E_g (Teeparthi et al., 2018). However, the E_g of ZrO_2 varies from 3.25 to 5.1 eV, dependent on the different preparation methods (Hassan et al., 2020; Kumar and Ojha, 2015). To date, various processes have been used to synthesize nano--ZrO_2, including sol-gel, hydrothermal, sonochemical, microwave irradiation, plant extract, PEO, anodization, and thermal plasma (Aziz et al., 2021; Maheswari et al., 2014).

Among those processes, the sol-gel method is a low-cost, low-temperature technology that does not necessitate the use of complex process equipment and provides good homogeneity and chemical purity. This method involves a soluble metal salt precursor, which acts as 'sol'. It gradually evolves towards forming a gel-like network containing both a liquid phase and a solid phase. During this process, the gel-like undergoes various forms of hydrolysis and polycondensation reactions. Specifically, ZrO_2 sol was produced from solvent (ethanol) into Zr precursors at 60 °C under 2 h of stirring. Then, the hydrolyzation process occurred by adding ammonia solution (pH 12) and continued stirring for 12 h. After that, the polycondensation happened by heating the solution until gel-formed before drying and calcination process. For example, Sultana et al. (2015) reported that ZrO_2 NPs were prepared by the sol-gel method. They found that nanostructured ZrO_2 with smaller particle sizes increased the photocatalytic activity of acid blue 25. Those approaches, however, have significant flaws, including a long reaction time and an uneven temperature distribution.

The hydrothermal and sonochemical method, a facile method, has been widely used to create innovative nanostructured materials. The former approach offers mild synthetic conditions, low pollution, and lower reaction temperature. Generally, under the hydrothermal method, the solution was transferred into a Teflon-lined stainless steel autoclave and heated at 120 °C for 6 h. After the cooling process, the white precipitate was washed and collected by centrifugation before it was dried and calcined. Shu et al., for example, used a hydrothermal method at 200 °C to make ZrO_2 nanostructures and discovered that ZrO_2 had high photoactivity for the MO degradation in both acidic and weakly basic water solutions when exposed to UV light (Shu et al., 2013).

For the sonochemical method, ultrasonic irradiation causes

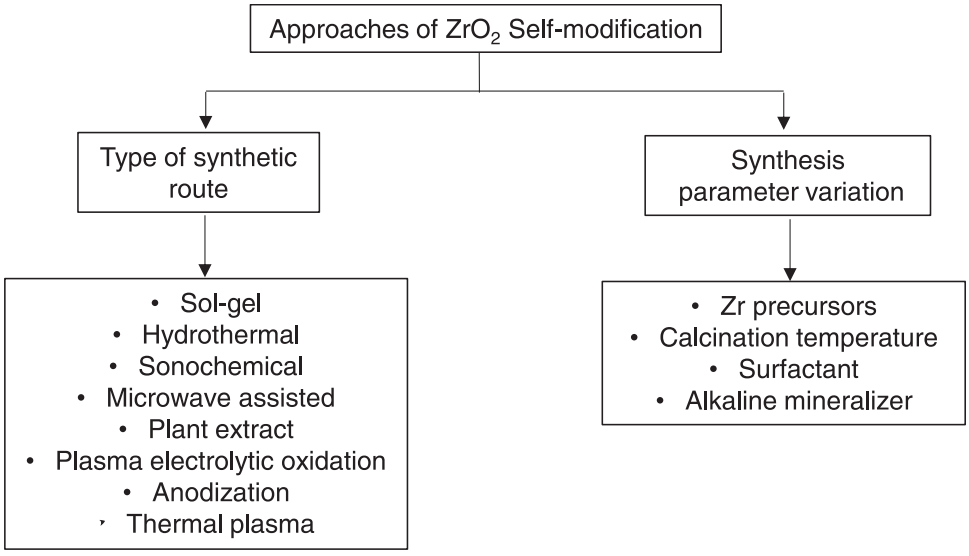

Fig. 2. Approaches of ZrO_2 self-modification.

cavitation in a liquid media, which causes implosive collapse as well as bubble formation. These bubbles with brief lives collapse, resulting in high pressure and strong local heating. These hotspots can generate extremely high temperatures and pressures, which are ideal for various chemical reactions. Briefly, Zr and ammonia (solvent) solution undergo ultrasonic irradiation before being cooled at room temperature. The solution was filtered, dried, and calcined at 600 °C for 4 h. For example, Zinatloo-Ajabshir and co-workers successfully synthesized ZrO_2 NPs by sonication method with the aid of zirconyl nitrate and ethylenediamine (Zinatloo-Ajabshir and Salavati-Niasari, 2016). This catalyst exhibited higher performance in the degradation of eriochrome black T (72%) after 2 h under UV light irradiation. However, both methods involve higher pressure and temperature, consuming higher energy and resulting in higher costs.

Microwave (MW)-assisted technologies have become a viable approach to produce nanomaterials such as TiO_2, ZnO, and Mn_2O_3 over the previous decade (Haghjoo et al., 2017). MW heating differs from traditional heating. Thermal energy is provided to the material's surface by radiant and convection heating and then transported to the bulk of the material via conduction. On the other hand, MW heating is the absorption of MW radiation followed by volumetric heating, which entails the transition of electromagnetic energy to thermal energy. As a result, rapid and consistent heating of the materials is achievable. Compared to the traditional approach, consistent and quick heating creates small particles with narrow size distribution and great purity. For example, Dwivedi et al. (2011) used an MW-assisted sol-gel method to synthesize *t*-ZrO_2 NPs. They exposed the mixture of Zr salts with citric acid and distilled water to MW for 2 min for evaporating before the white gel was ground and calcined.

Besides, recently, many researchers are focusing on the green, fast, appealing, and cost-effective production of metal oxide NPs by plant extract. Briefly, the mixture of plant extract and Zr aqueous solution was stirred, and subsequently, the evaporation process takes place by using a microwave oven at a higher temperature until the white powder was obtained (Shinde et al., 2018). The usage of plant extract could eliminate hazardous chemicals for synthesis materials. It is noted that plant extract was employed as a reducing and capping agent, preventing particle growth. This fact was proven by the produced ZrO_2 NPs show excellent performance in the elimination of MB and MO, with 91% and 69%, respectively, when *Ficus benghalensis* leaf extract is used as a capping agent in the synthesis of ZrO_2 NPs. Referring to Wu et al., which synthesized the ZrO_2 NPs by using green material, chitosan as a template. Briefly, the aqueous solution of chitosan in acetic acid was added into Zr solution with stirring until a precipitate formed before it was dried and calcined. The ZrO_2 powders using a lower molecular weight of chitosan with a higher surface area showed better efficiency of Rhodamine B (RhB) (86.2%) for 2 h (Wu et al., 2016).

Other than that, PEO, thermal plasma techniques, and anodization process are also used to prepare nano-ZrO_2. The main benefit of employing the PEO approach to make ZrO_2 films is that it takes a short amount of time and does not require additional thermal treatment. Furthermore, spark discharges occur on the surface, causing defects in the interfacial area (Tsai and Chou, 2018). Meanwhile, the anodization process formed the nano-size structure of metal-oxide in situ on the surface of the metal (Jiang et al., 2014). In this process, Zr foils, and platinum foils were used as anodic and cathodic electrodes. Before anodization, both foils will be cleaned ultrasonically in a mixture of distilled water, acetone, and ethanol. After that, both platinum foils were immersed in the electrolyte mixture, which contained fluorite solution (NH_4F and $(NH_4)_2SO_4$) and stirred vigorously. The anodization process was started by applying the voltage at 20 V under a specific time. Lastly, the sample was washed and dried overnight. This procedure was similar to the PEO, except for the electrolyte used, which was prepared using double distilled water and deionized water. Jiang et al. (2014) synthesized ZrO_2 nanocatalyst by anodization process using zirconium foil in an electrolyte containing NH4F and $(NH_4)_2SO_4$.

4.2. Synthesis parameters variation

Major aspects during synthesis, including the precursor, alkaline mineralizers, surfactants, and the calcination temperature, all influence the structure of ZrO_2 nanocrystals (Aminipoya et al., 2020). Many researchers used the cheap chemical CH_3COONa as a co-solvent in the preparation of ZrO_2 NPs. This solvent plays an essential role in the formation of ZrO_2 NPs with unique morphology. The NO_3^- had a significant influence on the development of ZrO_2 nanostructures since it prevents the contamination of the products. Meanwhile, CH_3COO^- anions tend to adsorb on the surface of ZrO_2. For example, Tao et al. (2018) synthesized nano-Zr using $Zr(NO_3)_4.5\ H_2O$ as a zirconium source with CH_3COONa for synthesized ZrO_2 nanocatalyst. Recently, more researchers focused on the synthesis of ZrO_2 NPs under different Zr precursors, including $ZrOCl_2{\cdot}8H_2O$ and Zr $(SO_4)_2{\cdot}4H_2O$ with the aid of CH_3COONa (Shu et al., 2012, 2013). Based on the previous study, the interaction of CH_3COO^- and Zr^{4+} ions with water molecules influences nanocrystal morphology. Thus, it can be concluded that different Zr precursors will form the different structures of ZrO_2 nanocrystal.

Besides, different calcination temperatures also influenced the properties of ZrO_2 nanocrystal. At higher calcination temperatures, the crystallites formed are larger, attributed to the thermally promoted crystallite growth. Thus, appropriate calcination temperatures exhibited suitable particle sizes for application in catalysis. Kumar and Ojha synthesized ZrO_2 NPs under different calcination temperatures at 500, 600, 700, and 900 °C (Kumar and Ojha, 2015). Based on the TEM images, the size of nanoparticles is increased by increasing the calcination temperature. Thus, the appropriate calcination temperature will enhance the catalytic performance.

Lastly, the sort surfactant and alkaline mineralizer significantly impact the phase stability of nanocrystals (Maheswari et al., 2014). On the other hand, surface-assisted synthesis of nano-inorganic materials has recently piqued interest due to its effective soft template effect, repeatability, and ease of mobility (Rezaei et al., 2006). Nanocrystalline *t*-ZrO_2 with high surface area and mesoporous structure could be synthesized utilizing a cationic surfactant, Pluronic P123 block copolymer with ethylenediamine as both a precipitating and colloidal protective agent (Rezaei et al., 2007). In fact, the different types of surfactants and mineralizers can influence the structure and physicochemical properties of the NPs by the degree of polymerization rate. Maheswari et al. (2013) found that the influence on phase change is mainly due to the number and rate of release of hydroxyl ions during polymerization. The polymerization rate for a strong base (NaOH) is faster than for a weaker one (NH_4OH). The gradual release of OH^- ions by NH_4OH limits the number of OH^- ions available to replace the OV in the lattice, allowing the *t*-ZrO_2 phase to stabilize.

As a summary of this section, the synthetic route is the prominent approach compared to the synthesis parameters for ZrO_2 self-modification. Several synthesis methods provide the exceptional properties of the catalyst, including smaller particle size and higher surface area that are beneficial for photocatalytic degradation of organic pollutants. Dominantly, MW is the facile and straightforward preparation method for nano-ZrO_2 catalysts. Most researchers focused on the variation of alkaline mineralizer and calcination temperature for the synthesis parameters since the phase changes more influence it.

5. Effect of ZrO_2 self-modification with enhanced photodegradation efficiency

The preparation and reaction conditions significantly impact the morphology, phase structure, and surface defect of synthetic nano-ZrO_2. Generally, those criteria influenced the photodegradation efficiency. Thus the discussion related to this matter was briefly explained in this section.

5.1. Morphology

The morphology of ZrO_2 has a considerable impact on its characteristics because it may manage physicochemical properties (Gao et al., 2011; Jaenicke et al., 2008). In recent years, many different approaches have been utilized to prepare ZrO_2 nanomaterials and the self-modification of ZrO_2 with different morphologies using suitable templates and surfactants. These approaches increased the efficiencies of photocatalytic performances. The nanomaterials are usually considered materials with at least one external dimension that measures 100 nanometres or less or with internal structures measuring 100 nm or less. They may be in the form of particles, tubes, rods, or fibers. Therefore, many reports have focused on the controlled preparation of ZrO_2 nanomaterials such as ZrO_2 nanoparticles, nanorods, nanowires, nanotubes, nanofibers, flower-like and star-like structures. Table 3 shows the different synthetic routes of various structures or morphology of ZrO_2 nanomaterials.

Generally, ZrO_2 exhibited in nanoparticles structure when using the sol-gel method. The nanoparticles induced a higher surface area, which enhanced the adsorption affinity and more active sites, thus improving catalytic performance. For example, Kumar and Ojha synthesize the ZrO_2 nanostructure with smaller particle sizes by the simple sol-gel method for degradation of MB (Kumar and Ojha, 2015). Similarly, nanostructured ZrO_2 thin film prepared by sol-gel method reached about 85% after 1 h, indicating superior photocatalytic activity towards MO degradation (Majedi et al., 2016). Jalil et al. (2015) reported a rapid and straightforward electrochemical method for preparing ZrO_2 nanoparticles. This smaller ZrO_2 crystal size showed a good performance in degrading the MB about 83.6%. Other than that, Mahmood et al. (2013) also successfully synthesized *t*-ZrO_2 nanoparticles by the sol-gel method. They found that the smaller crystallite size and greater OV explain the stability of the *t*-ZrO_2 phase.

Besides that, flower-like ZrO_2 nanomaterials, for example, with their unique form, synthesized under different Zr precursors, demonstrated outstanding photodegradation of RhB (Shu et al., 2012) (Fig. 3). Shu et al. (2013) also used a hydrothermal synthesis approach to produce star-like *t*-ZrO_2 nanostructures using $ZrOCl_2{\cdot}8H_2O$. The catalyst degraded MO entirely in 1 h under both acidic and weak basic solutions. Because of the distinctive exposed feature of the hierarchical structure of ZrO_2, the flower-like ZrO_2 nanostructures show excellent photocatalytic activity. Similarly, Tao et al. (2018) employed $Zr(NO_3)_4{\cdot}5\ H_2O$ as a zirconium source and created star-like ZrO_2 by a hydrothermal process without the need of a template or surfactant. The photocatalytic activity of the produced ZrO_2 was superior, with a narrow E_g, which is 3.50–3.85 eV, and almost 100% destruction of RhB in 30 min. Besides, the hierarchical structure of *m*-ZrO_2 nanorods was prepared by Khan et al. (2014) using the hydrothermal method. Meanwhile, Taguchi et al. (2014) used subcritical hydrothermal conditions to make single-phase *m*-ZrO_2 nanocrystals.

The shortest dimension for efficient e^- transport and optical stimulation is one-dimensional nanostructures, including nanotubes and nanowires (Fig. 4). Cao et al. (2004) report on the preparation of ZrO_2 nanowires by a template method and their optical properties. Jiang et al. (2014) synthesized ZrO_2 nanotubes by anodization process using zirconium foil in an electrolyte containing NH4F and $(NH_4)_2SO_4$. The researchers found that ZrO_2 nanotubes had exceptional photocatalytic performance, with a 94.4% MO photodegradation rate after 240 min. They also asserted that the hydroxyl group absorption on the surface was responsible for photocatalysis performance. In addition, this process itself generates·OH free radical to oxidize the adsorbed MO and subsequently increased the photoactivity. The photodecolorization of methyl red was also improved by self-organized nanoporous *t*-ZrO_2 arrays with excellent adherence to the Zr substrate (Wierzbicka et al., 2021).

Fang et al. (2013) showed the photocatalytic activity of ZrO_2 nanotubes towards MO dye at a higher pH value. When the diameter of ZrO_2 nanotubes is increased, the rate of dye degradation increases. Nanotubes arrays have a large surface area, increasing the adsorption affinity towards model pollutants and increasing the photoactivity. Zhao et al. synthesized ZrO_2 nanotubes with an inner diameter (80 nm) and a wall thickness (35 nm) using anodization. The authors discovered a 97.6% MO decolorization percentage at a pH value of 2 (Zhao et al., 2011). Ismail et al. (2011) created a 6 nm thick oxide coating with a ZrO_2 nanotubular, and the authors investigated the ZrO_2 nanotubes' photocatalytic activity. After 120 min of reaction, the authors reported that 30% MO degradation over *t*-ZrO_2 nanotubes was in the presence of UV light.

The mesoporous structured photocatalyst appears to be more promising due to larger surface area and multiple scattering. Lately, Mobil scientists had successfully prepared the silica-based mesoporous material and offered new possibilities for producing mesoporous ZrO_2 with a high surface area (Sreethawong et al., 2013; Carević et al., 2016) (Fig. 5A). TEM images show the intercluster mesoporous voids

Table 3
Different synthesis methods of various structure of ZrO_2 nanomaterials.

Photocatalyst shape	Synthesis method	Degradation (%)	Pollutant	References
ZrO_2 nanoparticles	Sol-gel	65.0, 75	Acid Blue 25	Sultana et al. (2015)
t-ZrO_2 nanoparticles	Sol-gel	35.0, 60	Methylene blue	Kumar and Ojha (2015)
ZrO_2 nanoparticles	Sol-gel	85.0, 60	Methyl Orange	Majedi et al. (2016)
t-ZrO_2 nanoparticles	Sol-gel	n.a	n.a	Mahmood et al. (2013)
Mesoporous ZrO_2 nanoparticles	Sol-gel	68.4	Methyl orange	Sreethawong et al. (2013)
ZrO_2 nanoparticles	Sol-gel	76.0, 300	Methylene Blue	Teeparthi et al. (2018)
Flower-like ZrO_2	Hydrothermal	100, 80	Rhodamine B	Shu et al. (2012)
Star-like ZrO_2	Hydrothermal	100, 120	Rhodamine B	Shu et al. (2013)
Star-like ZrO_2	Hydrothermal	100, 30	Rhodamine B	Tao et al. (2018)
t-ZrO_2 nanoparticles	Hydrothermal	99.0, 50	Methyl orange	Reddy et al. (2018)
ZrO_2 nanoparticles	Sonochemical	72.0, 120	Eriochrome Bnack T	Zinatloo-Ajabshir et al., 2016
ZrO_2 nanoparticles	Electrochemical	83.6, 240	Methylene blue	Jalil et al. (2015)
ZrO_2 nanoparticles	Microwave	n.a	n.a	Dwivedi et al. (2011)
ZrO_2 nanoparticles	Plant extract	91.0, 240	Methylene blue	Shinde et al. (2018)
ZrO_2 nanoparticles	Plant extract	86.2, 120	Rhodamine B	Wu et al. (2016)
ZrO_2 nanoparticles	Thermal plasma	100, 30	Methylene blue	Nawale et al. (2012)
ZrO_2 nanotubes	Anodization	94.5, 240	Methyl orange	Jiang et al. (2014)
ZrO_2 nanotubes	Anodization	94.6, 240	Methyl orange	Zhao et al. (2011)
ZrO_2 nanotubes	Anodization	n.a	n.a	Ismail et al. (2011)
ZrO_2 nanotubes	Anodization	30, 120	Methyl orange	Fang et al. (2013)
Nanoporous-ZrO_2	Anodization	95.3, 300	Methyl red	Wierzbicka et al. (2021)
Fibrous ZrO_2	Microemulsion	96, 180	Chromium (VI)	Aziz et al. (2021)

t = tetragonal phase, n.a=not available

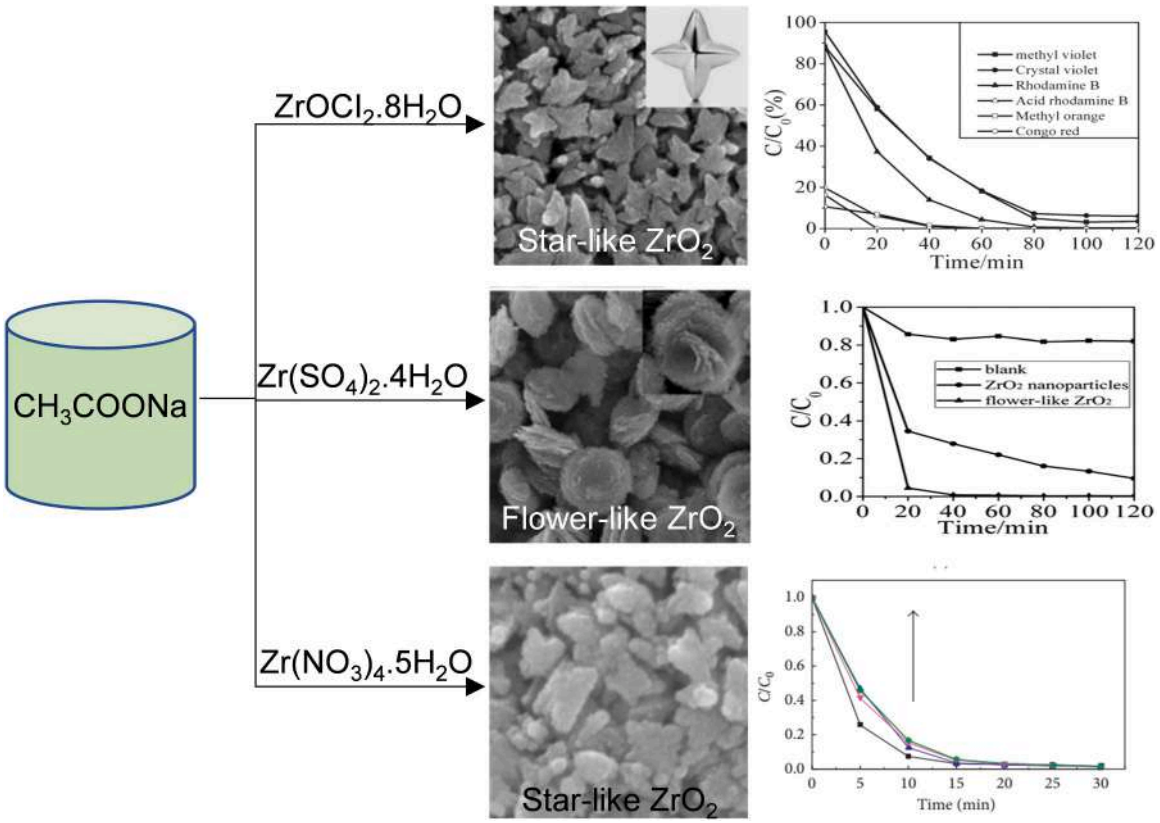

Fig. 3. Preparation of star-like and flower-like ZrO2using different of Zr salts under hydrothermal method and their performances indegrading the dye. Adapted from Shu et al. (2012, 2013) and Tao et al. (2018).

formation (Fig. 5B). This catalyst's increased degradation percentage could be attributed to its mesoporous structure, which allows for greater reactant accessibility to the surface active sites and more efficient multiple light scattering inside the mesopore channel (Fig. 5C). For the production of mesoporous ZrO_2, two mechanisms exist a templating mechanism and a scaffolding mechanism. The system's templating mechanism produces materials with well-ordered pore systems and vice-versa for scaffolding mechanism, which involves disordered pore arrangement of mesoporous material (Deshmane and Adewuyi, 2012). Based on these stated techniques, a thorough examination of past literature offers several approaches for preparing mesoporous ZrO_2.

Soft templating with a surfactant is another method that enables micro-mesopores' creation with dendrimer silica fiber architectures nowadays. Polshettiwar et al. were the first to use fibrous silica materials, which are today known as KAUST Catalysis Center (KCC-1) catalysts. The inclusion of dendrimer silica fibers on KCC-1 boosted the accessibility of the active sites, resulting in better catalytic activity (Fauzi et al., 2018; Fatah et al., 2017). Aziz et al. (2021) used a microemulsion method to synthesize fibrous silica zirconia, FSZr (Fig. 6A). HRTEM image shows the dendrimer fibers of ZrO_2 (Fig. 6B). Compared to commercial ZrO_2, the FSZr catalyst showed superior photoactivity, with 59% of pC photooxidation and 96% photoreduction of Cr (VI) under visible light irradiation (Fig. 6C). This is due to its structural features, which include crystallinity, pore volume, and surface area.

5.2. Crystal structure

In general, the phase transitions and crystalline structure of ZrO_2 catalysts greatly impact their uses. ZrO_2 has three distinct crystalline forms at atmospheric pressure: *m*-ZrO_2 (< 1170 °C), *t*-ZrO_2 (>1170 °C< 2370 °C), and *c*-ZrO_2 (> 2370 °C). Furthermore, *m*-ZrO_2 (270 cm^{-1}), *t*-ZrO_2 (435 cm^{-1}) and *c*-ZrO_2 (480 cm^{-1}) structures have different infrared frequencies. This means that the crystalline structure of ZrO_2 is dependent on its optical phonon energy (Dwivedi et al., 2011).

Many researchers' key focus was on the *t*-ZrO_2 as an active photocatalytic material for phenolic compound degradation due to its active surface and smaller particle size (Hassan et al., 2021a). However, the *t*-ZrO_2 is thermodynamically stable at higher temperatures. At low temperatures, *t*-ZrO_2 can be stabilized by two approaches: decreasing the grain size to a nanometer or incorporating dopants to introduce defects in the lattice. For example, Jalil et al., synthesized *t*-ZrO_2 at a lower calcination temperature without adding a dopant in the preparation step (Jalil et al., 2015). It was suggested that the use of tetraethylammonium perchlorate as the supporting electrolyte was responsible for the stabilization of *t*-ZrO_2 by preventing the agglomeration of metal clusters with undesired powders in the electrolysis system, resulting in a decrease in ZrO_2 crystal size. This catalyst facilitated good photoactivity towards MB degradation (83.6%) under UV light in a batch reactor compared with commercial ZrO_2 (58.7%) and Degussa P25 TiO_2 (64.5%).

Other than that, Reddy et al. (2018) was successfully synthesized *t*-ZrO_2 using the hydrothermal method. The smaller size of crystallite indicates the existence of OV at the surface and grain boundaries. The presence of OV will prevent the growth of the nanoparticles and produce a stress field. The created defects will act as a scattering center for e^-, h^+ and stimulate the recombination of the e^--h^+ pairs that influence photocatalytic activity and photoluminescence performance. Results showed that 99% degradation was achieved within 50 min under UV light irradiation.

The crystalline structure of *t*-ZrO_2 nanoparticles was confirmed by X-ray diffraction (XRD) analysis, with a prominent peak at $2\theta = 30.0°$, related to the (101) plane. Other than that, the photoluminescence (PL) technique is a suitable method to determine the crystalline quality, presence of impurities, and exciton fine structure. In fact, the high

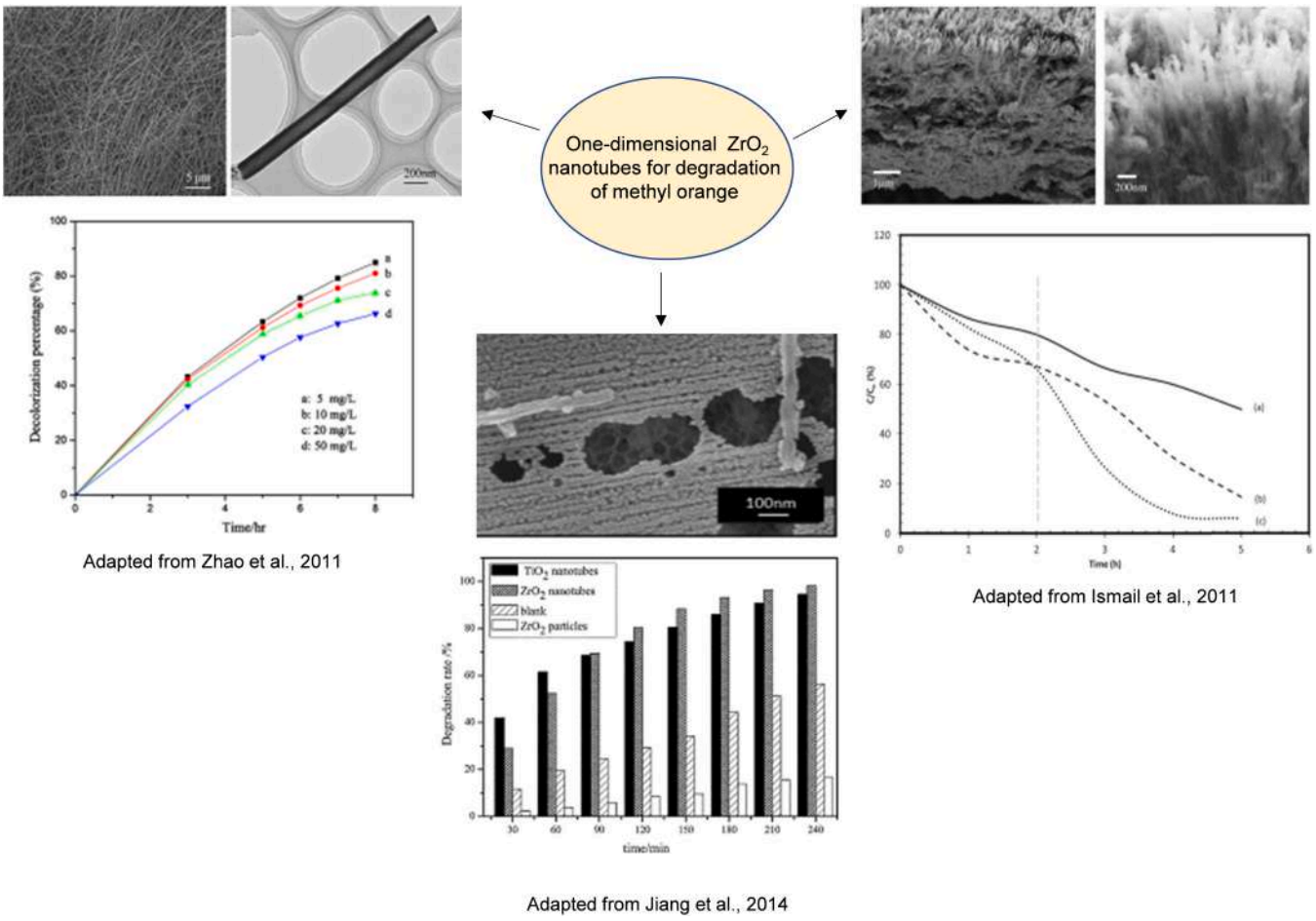

Fig. 4. ZrO_2 nanotubes formed by anodization process for degradation of methyl orange.

crystallinity is related to the smaller crystallite size, which indicates that OV's existence at the surface and grain boundaries. From the PL spectrum, the green emission band (537 nm) shows the surface defects, particularly OV in the ZrO_2 lattice. Due to the high crystal quality of the ZrO_2 catalyst, the visible emission in ZrO_2 nanostructures can be associated with the surface defect. Thus, it can be concluded that the presence of OV and higher crystallinity ZrO_2 offered a strong ability for photocatalytic reaction under visible light irradiation.

In previous research, high crystalline mesoporous ZrO_2 has been synthesized for photocatalytic dye degradation compared to that of the P25 TiO_2 nanoparticles for the MO dye degradation (Sreethawong et al., 2013). The synthesized ZrO_2 nanoparticles exhibited high crystallinity due to the intensity sharpness of all the dominant diffraction peaks, as confirmed by the XRD spectrum. This crystalline mesoporous ZrO_2 shown a greater MO degradation under optimum conditions. It is due to the combination between the mesoporous-assembled structure and the higher specific surface area of the synthesized ZrO_2 nanoparticles is reasonably hypothesized to bring about a higher degradation activity.

Basahel et al. (2015) found that pure *m*-ZrO_2, *t*-ZrO_2, and *c*-ZrO_2 photocatalysts demonstrated 99%, 90%, and 80% degradation of MO in 110, 90, and 240 min, respectively with different E_g (Fig. 7A). The result shows that the crystal structure of ZrO_2 influenced the photocatalytic degradation of MO. In this study, the researchers used Raman spectroscopy to confirm the crystalline structure of the ZrO_2. It is because the *c*- and *t*-ZrO_2 structures, based solely on the XRD analysis, can be misleading because the *c*- and *t*-ZrO_2 structures (a_0 = 0.5124 nm for *c*-ZrO_2 and a_0 = 0.5094 nm and c_0 = 0.5177 nm for *t*-ZrO_2 structures) are very similar. So, from Raman spectra, the *m*-ZrO_2 sample showed several peaks centering at 183, 301, 335, 381, 476, 536, 559, 613, and 636 cm^{-1}. While the *t*-ZrO_2 sample showed peaks at 149, 224, 292, 324, 407, 456, and cm^{-1}. And, the Raman spectrum for *c*-ZrO_2 is characterized by a narrow band at 145 cm^{-1} and broad bands centered at 246, 301, 436, and 625 cm^{-1}. Other than that, to authenticate the ZrO_2 phase in the samples, high-resolution transmission electron microscopy (HRTEM) was carried out on particles of the three samples. It was found that the distance between the fringes was calculated to be 0.297 nm, 0.296 nm, and 0.291 nm, which can be attributed to the interplanar spacing corresponding to (111) plane of *m*-ZrO_2, *t*-ZrO_2, and *c*-ZrO_2, respectively.

The study regarding phase-controlled ZrO_2 is a crucial topic to investigate due to the numerous technological uses of different phases of ZrO_2. Many researchers have investigated the impact of thermal treatment on the morphology and crystal structure of ZrO_2 NPs (Nawale et al., 2012). At 700 °C, Rashad and Baioumy stated that the co-precipitation technique produced *t*-ZrO_2 with low crystallinity, but that the *t*-ZrO_2 was converted to *m*-ZrO_2 at temperatures ranging from 1000° to 1200°C (Rashad and Baioumy, 2008). Meanwhile, the citrate gel combustion approach resulted in the development of *m*-ZrO_2 without the presence of *t*-ZrO_2 in the temperature range between 1000 and 1200 °C. Compared to the other approaches at 700 °C, the microemulsion improved precipitation technique resulted in the development of a *t*-ZrO_2 with good crystallinity. At calcination temperatures of 1000–1200 °C, however, the *t*-ZrO_2 was converted into the *c*-ZrO_2. According to Ward and Ko, ZrO_2 aerogel can be fully amorphous, *t*-ZrO_2, or *m*-ZrO_2, depending on the heat treatment (Ward and Ko, 1993). At temperatures above 400 °C, Santos et al. (2008) discovered a *t*-ZrO_2, which changes into an *m*-ZrO_2 above 600 °C. It has also been stated that OV plays a crucial role in determining the system's final crystalline

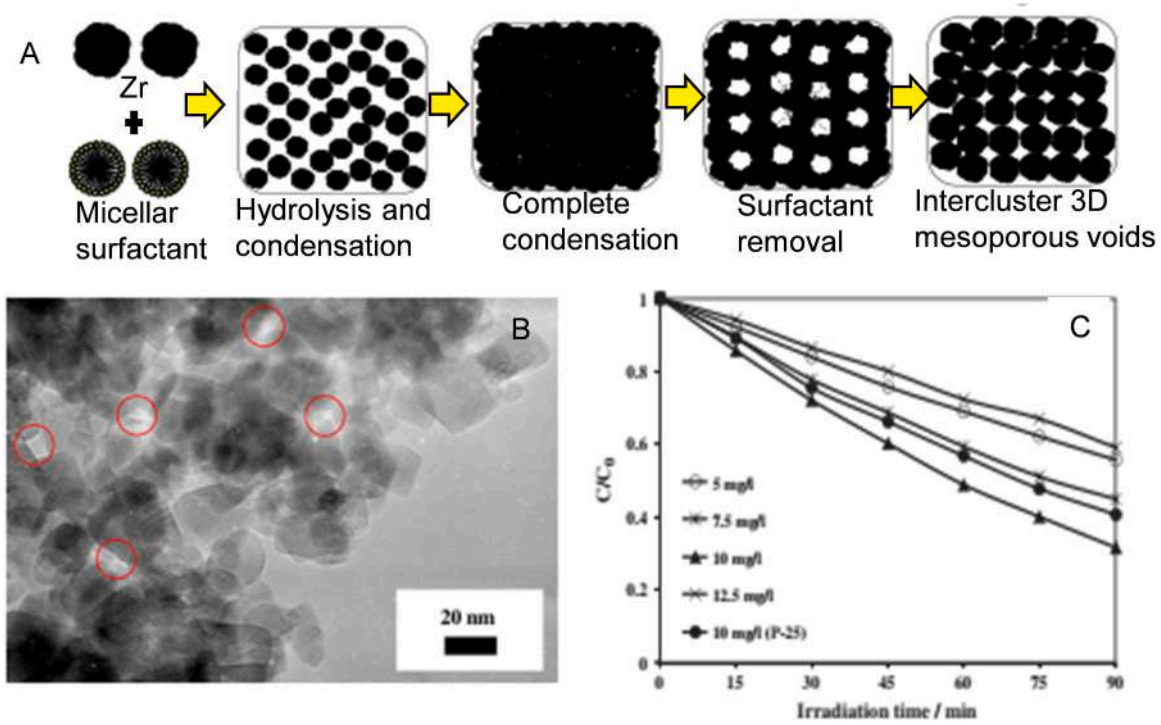

Fig. 5. (A) Proposed model of the mesopore formation by using sol-gel, (B) High-resolution TEM image for the mesoporous ZrO2 and (C) Photoactivity of MO degradation over mesoporous ZrO2.
Adapted from Sreethawong et al. (2013).

phase.

For the case studies by Wierzbicka et al., as-synthesized anodic ZrO_2 are already crystalline and, therefore, do not require further thermal treatment to provide high photocatalytic performance (Wierzbicka et al., 2021). However, photocatalytic efficiency could be improved by annealing at a relatively low temperature of 350 °C. Higher annealing temperatures caused a gradual drop in photocatalytic activity. The photocatalytic behavior was correlated with the crystal phase transformation in anodic ZrO_2. It was found that higher photocatalytic activity was observed for the *t*-ZrO_2 over the *m*-ZrO_2 (predominant at elevated temperatures). It results from the optimal and complex electronic structure of annealed ZrO_2 with three different energy states having absorption edges at 2.0, 4.01, and 5.28 eV.

5.3. Surface defects

Defect, in general, refers to the deviation of the actual crystal structure from the ideal lattice structure. There are many defects, including point defects, line defects, interface defects, and bulk defects. Solid materials, particularly nanomaterials with small dimensions, are prone to defects. Defect structures are simply designed to synthesize or modify nanomaterials due to their high surface energy (Xie et al., 2020). In particular, the self-modification by generating defect structures of ZrO_2 is crucial for enhanced catalytic performance and is briefly discussed in this section.

According to solid-state defect chemistry, defects in catalysts can produce more unsaturated coordination sites, which promote reaction molecule adsorption. Indeed, defect structures can be used as adsorption sites to boost catalytic performance. Therefore, several investigations have been conducted to boost catalytic performance and address the demand for novel visible-light-driven materials by adding surface defects. OV is the most prevalent defect type in transition metal oxides, which plays a critical role in heterogeneous photocatalysis. Furthermore, by supplying extra energy levels, particularly near the Fermi Level, and serving as reactive sites, these vacancies play a crucial role in changing the properties of photocatalysts (Niu et al., 2014).

It was observed that creating surface defects and OV in ZrO_2 under magnesiothermic reduction (5% H_2/Ar) resulted in a significant increase in photocatalytic (Sinhamahapatra et al., 2016). Under simulated solar light, they found that the OV-rich black ZrO_{2-x} (BZ, 1.55 eV) has strong catalytic performance for photodegradation of RhB and H_2 generation. The existence of substantial OV and Zr^{3+} in BZ compared to white ZrO_2 can be attributed to the significant change in E_g due to the development of new energy states around CB and VB (WZ, 5.14 eV). The Zr^{3+} produced by OV contributes primarily to the CB tail, as evidenced by the density of states of the Zr 4d band. These Zr^{3+} can effectively limit e^--h^+ recombination, allowing sunlight to be absorbed across a larger spectrum of wavelengths, including visible light. Unlikely, Teeparthi et al. (2017) stated that despite the presence of OV, BZ exhibited relatively little activity due to the existence of the *t*-ZrO_2, as well as the insufficient development of new states level in the VB and CB as they approached the Fermi energy level. As a result, even if there is defect chemistry, the altered crystal structure also validated the tetragonal phase's negative function in visible light photocatalytic activity.

Besides that, different calcination temperatures of ZrO_2 also influenced the generation of OV. Kumar and Ojha reported that room temperature ZrO_2 nanostructure was synthesized by simple sol-gel method and calcined at 500 °C, 600 °C, 700 °C, and 900 °C (Kumar and Ojha, 2015). As the calcination temperature was increased, the PL intensity decreased, which was attributed to the lower number of defects centers, including OV/Zr vacancies/Zr^{3+} interstitials. These properties could be the reason for lowering the catalytic efficiency in degrading the MB dyes. The more significant OV played a crucial role in decreasing the E_g and creating photocatalysis active or trap centers (Guo et al., 2011). From the study, ZrO_2 (500 °C), which possessed the highest OV, showed excellent performance (Fig. 7B). Thus, it may be established that varied OV concentrations result in various light absorption capacities and photocatalytic activity.

Another method in generating the OV is PEO. PEO time influenced the concentration of OV, which longer PEO process was led to the

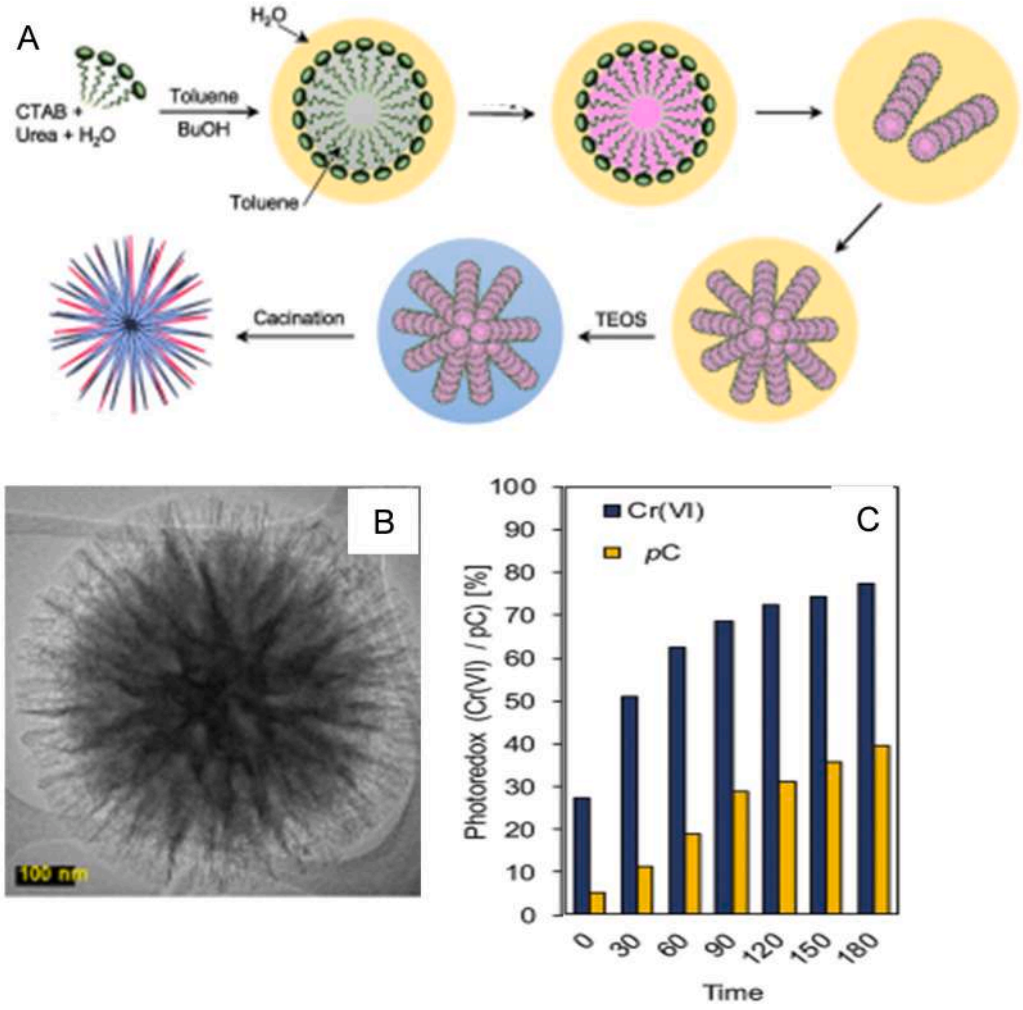

Fig. 6. (A) Proposed model of fibrous morphology, (B) HRTEM image and (C) Catalytic activity of photo-reduction of Cr(VI) and photo oxidation of cresol by fibrous zirconia.
Adapted from Fauzi et. al (2018) and Aziz et al. (2021).

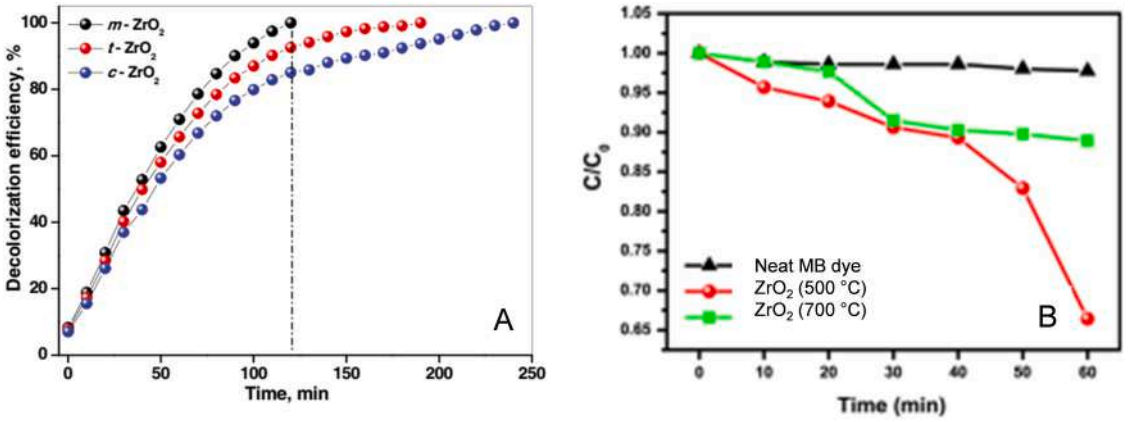

Fig. 7. Decolorization efficiency of (A) methyl orange in the presence of different phase structure of ZrO2 and (B) methylene blue under different calcination temperature.
Adapted from Basahel et al. (2015) and Kumar and Ojha (2015).

thicker ZrO_2 films that create a higher number of OV defects within oxide film, thereby contributing to the higher photocatalytic activity (Stojadinović et al., 2015). Nawale et al. (2012) also described the highest photoactivity of ZrO_2 nanostructure, in which the catalyst was prepared by thermal plasma method at 1.33 bar. The existence of OV inhibits the growth of NPs by applying a stress field. These defects will operate as a scattering center for e^- and h^+, causing e^--h^+ pairs to recombine, affecting the photocatalytic activity and photoluminescence

performance (Nagaveni et al., 2004). However, the excess of OV generally acts as a recombination center, which affected the performance. Thus, it is critical to have an optimal concentration of defects to improve photoactivity efficiency.

The hydrothermal process has been used to synthesize OV-rich ZrO_2. Reddy et al. (2018) successfully synthesized pure ZrO_2 by hydrothermal method. This catalyst was used for the degradation of MO with 99% for 50 min. The higher photoactivity is mainly ascribed due to the higher surface area as well as surface defects. Similarly, Basahel et al. (2015) synthesized OV-rich ZrO_2 under higher temperature (180 °C), and the catalyst degraded MO with 100% efficiency in 4 h. Meanwhile, Zhang et al. (2018) reported that OV-rich ZrO_2 nanocrystals synthesized by solvothermal method at 220 °C enhanced the photodegradation of TCH with 80% in 150 min. Specifically, this catalyst, in particular, contains highly charged OV (·OV and··OV), which suppressed the e^--h^+ pairs recombination subsequently enhanced the photocatalytic degradation of TCH.

The OV•, OV••, and OV× are the three types of OV found in metallic oxide (Gionco et al., 2013). OV× denotes that one OV contains two e^-, unaffected by the presence of O_2^- site. Meanwhile, OV• represents that one OV has one e^-, resulting in a singly charged OV, while another e^- from the OV site binds to a nearby Zr^{4+} ion, forming a Zr^{3+} ion. One OV without e^- forms a doubly charged OV denoted by OV••), in which two e^- locate at two neighboring Zr^{4+} ions and produce two Zr^{3+} ions. Interestingly, the position of VB is discovered to be necessary. After annealing at 350 °C, it drops from ~2.63 eV to ~2.86 eV and then rises to ~ 2.65 eV after annealing at 520 °C. The amount of the charged OV and Zr^{3+} should be connected to the change in VB's location (Gorban et al., 2015).

Recently, the MW approach, which involves rapid heating rates, short processing times, homogeneity, and low power requirements, is the ideal approach for synthesizing a sample of defect-free particles (Dwivedi et al., 2011). OV was formed due to the polycondensation reaction of Zr precursors during MW heating, which more O was removed as a consequence of well condensation. At the same time, the produced e^- were trapped on the Zr^{4+} sites, forming Zr^{3+} (Gionco et al., 2015; Hassan et al., 2018a, 2021b). The relatively consistent heat distribution additionally boosted the OV quantity. Singh et al. (2014) used a microwave-assisted chemical technique to make ZrO_2 NPs at 80 °C. Because of their great surface area, they found that the as-synthesized nano-ZrO_2 particles have many surface defects. These characteristics suggest that visible-light-driven photocatalytic processes have a lot of promise.

Zheng et al. (2009) used the L-lysine-assisted hydrothermal technique to produce ZrO_2 nanoparticles with an average particle size of 8 nm, and their photocatalytic activity under UV irradiation was investigated on RhB dye. They discovered that the density of OV on the nanostructures' surfaces enhanced the photocatalytic activity of ZrO_2. Similarly, the catalytic activity of ZrO_2 nanoparticles also was investigated by Sato and Kadowaki. (Sato and Kadowaki, 1987). They explained that the development of an impurity band at 320 nm enhanced the photocatalytic activity over ZrO_2 nanostructures. Thus, it can be concluded that the OV derived from self-modification could improve the catalytic performance by suppressing the recombination of e^--h^+ pairs.

In conclusion, the synergistic effects of all three properties through self-modification could enhance the efficiency of photodegradation of organic pollutants. Different morphology was led to the further concentration of OV and phase change. In terms of the amount or concentration of OV, the excess of the OV could lead to the lower catalytic activity as it becomes a recombination center. Thus, an appropriate amount of OV could enhanced the photocatalytic activity.

6. Photocatalytic mechanism involves ZrO_2 self-modification

The mechanism of photodegradation of organic pollutant, for example, is TCH, were discussed on detail for pure ZrO_2 without (no self-modification) and with OV, OV-ZrO_2 (self-modification) (Zhang et al., 2018). As shown in Fig. 8, when visible light is irradiated to the catalyst, the e^- will be excited to CB and leaving h^+ at VB. Since e^- was unstable at an excited state, e^- will be jumped back into the VB and recombine with h^+ (case for ZrO_2). As the OV and Zr^{3+} formed from self-modification and acted as an e^- trapper, the e^- was transferred to the OV. This occurrence could significantly improve the photoactivity of OV-ZrO_2 compared to ZrO_2 by suppressing the recombination rate of e^--h^+ pairs. In these circumstances, the e^- played a role in reduced O_2 into·O_2^-, whereas the h^+ reacted with H_2O to form·OH, and in parallel, h^+ also oxidized the TCH into carbon dioxide and H_2O. The following is a list of reactions:

$$ZrO_2 - TCH \xrightarrow{hv(\lambda>420nm)} ZrO_2 - TCH^{\bullet +} + e^- \quad (8)$$

$$e^- + OV^{\bullet\bullet} \rightarrow OV^{\bullet} \quad (9)$$

$$e^- + OV^{\bullet} \rightarrow OV^{\times} \quad (10)$$

$$OV^{\bullet} + O_2 \rightarrow OV^{\bullet\bullet} + {}^{\bullet}O_2^- \quad (11)$$

$$OV^{\times} + O_2 \rightarrow OV^{\bullet} + {}^{\bullet}O_2^- \quad (12)$$

$$ZrO_2\text{–}TCH^{\bullet +} \rightarrow ZrO_2 + degraded\ products \quad (13)$$

$$TCH + {}^{\cdot}O_2^- \rightarrow degraded\ products \quad (14)$$

Another mechanism for the self-modification of ZrO_2 with surface defects, OV under UV light, is explained with the aid of a schematic diagram as shown in Fig. 9. The PL spectroscopy can confirm the generation of OV. The emission band at 401 nm has resulted from the radiative recombination of a photogenerated h^+ with an e^- occupying the OV. When excitation energy exceeds the bandgap of ZrO_2 nanostructures, e^--h^+ pairs are produced. The e^- are trapped very quickly by the OV that creates F centers. The Zr^{4+} ions adjacent to the bulk OV could capture electrons resulting in the formation of Zr^{3+} ions. Recombination of the h^+ with the F centers creates the excited states of the emitter. These exciting emitters undergo radiative transitions to the ground state. The recombination process can be described using the following equations:

$$ZrO_2 + hv \rightarrow e^- + h^+ \quad (15)$$

$$OV + e^- \rightarrow F \quad (16)$$

$$F + h^+ \rightarrow (OV)^* \rightarrow OV + hv \quad (17)$$

The main source of defects centers in ZrO_2 is OV/interstitial, Zr vacancies/interstitials (Zr^{3+} interstitials). As presented in Fig. 9, when UV light is incident on MB dye suspension, the e^--h^+ pairs are generated due to the ejection of e^- from VB that creates an h^+ in the VB. In this case, e^- only excited to defect centers but not to CB since the applied of UV light. These generated h^+ are allowed to react with OH ions and e^- may react with dissolved O_2 and creates the·OH radical into the aqueous solution. The complete mechanism for degradation of MB dye can be understood with following chemical reaction with ZrO_2:

$$ZrO_2 + hv \rightarrow ZrO_2 + e^- + h^+ \quad (18)$$

$$OH^- + h^+ \rightarrow OH^{\bullet} \quad (19)$$

$$O_2 + e^- \rightarrow O_2^- \quad (20)$$

$$O_2^- + H^+ \rightarrow HO_2 \quad (21)$$

$$2HO_2 \rightarrow H_2O_2 + O_2 \quad (22)$$

$$H_2O_2 + e^- \rightarrow OH^{\bullet} + OH^- \quad (23)$$

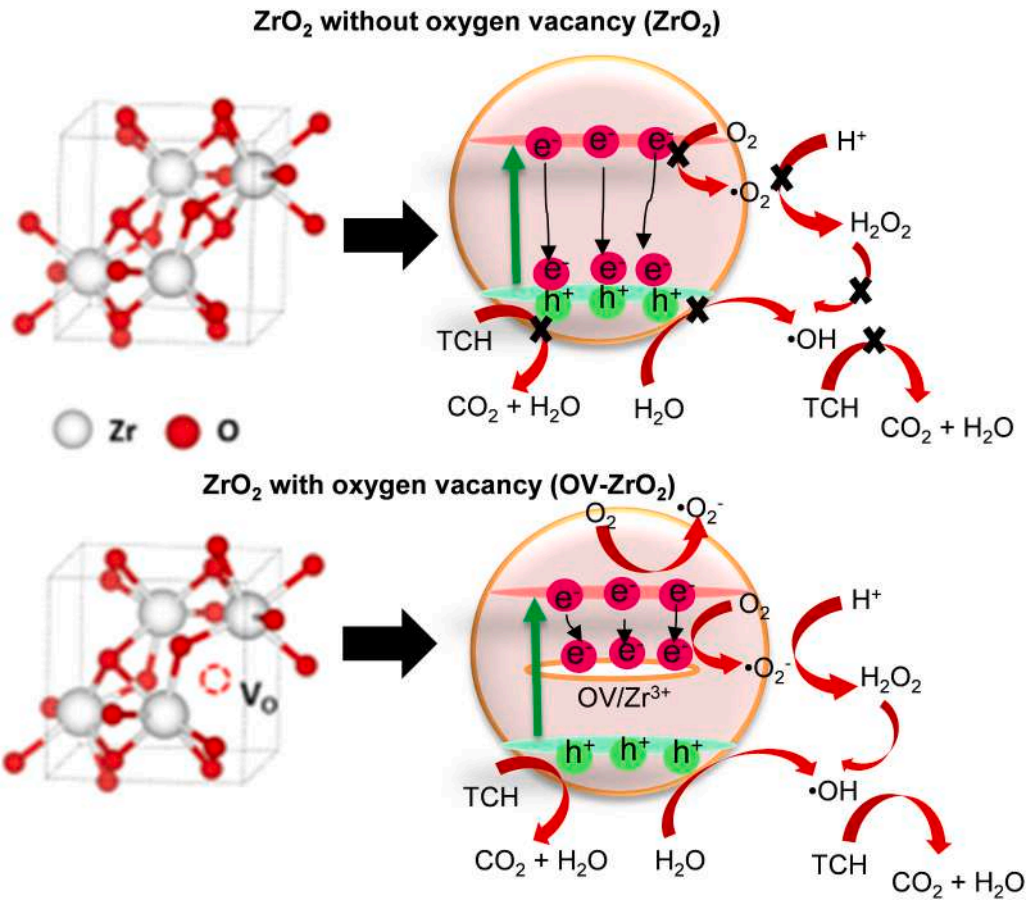

Fig. 8. Crystal structure and photocatalytic mechanism of ZrO_2 without oxygen vacancy and with oxygen vacancy under visible light irradiation.

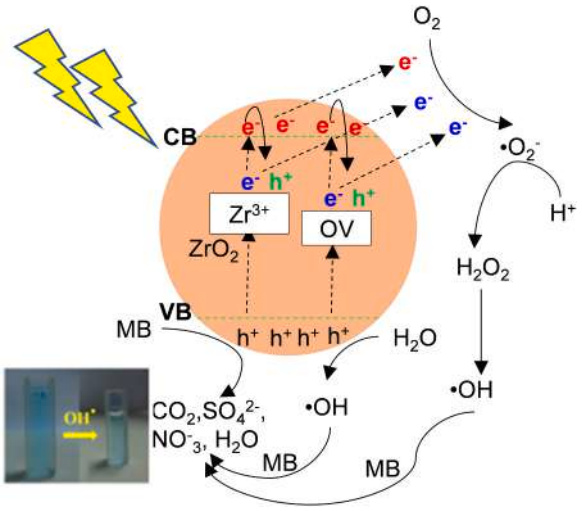

Fig. 9. Photocatalytic mechanism of ZrO_2 for degradation of MB under UV light.

Generally, two oxidative agents can be considered (i) the photo-produced h^+ (mainly involved in the decarboxylation reaction) (ii) the·OH radicals. These agents are known as strong, active degrading agents. In this present case, h^+ may not be considered a degradation agent since the reactant taken in the present study is cationic in nature. Thus, the·OH radicals can attack to C-S^+=C functional group of MB dye attached through coulombic interaction with the surface of ZrO_2 nanostructures. After the degradation of the MB dye, CO_2, SO_4^{2-}, NO^-_3, H_2O, and H^+ are found as the final products.

In conclusion, the OV was beneficial for enhanced the photocatalytic activity of ZrO_2 under UV and visible illumination since it can suppress e^--h^+ pairs. However, the roles of OV are different under UV and visible light, in which the OV acts as an e^- transporter as the higher energy needed to excite e^- directly to CB under UV illumination. Unlikely, e^- easily excited to the CB under visible illumination, and the e^- was unstable at excited state or CB. Subsequently, the e^- was transferred to the OV as it can act as an e^- acceptor. Therefore, the OV plays a crucial role in enhancing the photocatalytic activity of ZrO_2 under UV light and visible light.

7. Advantages and disadvantages of self –modification

Nowadays, modifying the photocatalyst is an effective method for enhanced catalytic performance. A significant necessity for optimizing ZrO_2's solar light harvesting performance is the alteration of its band structure. To decrease the E_g of ZrO_2 and broaden its light absorption range, researchers used self-modification and extra-modification as a generic technique for tweaking semiconductor E_g. As ZrO_2-like photocatalysts have a large E_g, increasing the spectrum responsiveness through self-modification may reduce the chances of recombination. Commonly, OV generated from many synthetic routes could suppress the recombination by acting as an e- acceptor and narrowing the E_g. In addition, OV also can act as an e^- transporter, which only used lower photon energy for e^- excitation.

In comparison to the extra-modification, the doped elements, in particular, operated as recombination centers for produced h^+ and e^-, which is detrimental to the photocatalytic activity. In addition, the blockage of light reduced the efficiency in degrading the organic pollutants due to doped elements. Furthermore, the possible toxicity of

doped elements is a significant concern, especially when using metal dopants. However, self-modification has its limitation. For example, due to the down-shift of CB, narrowing the E_g of the catalyst via self-modification typically comes at the expense of lowering the reduction capacity of the e^-. In conclusion, self-modifying is a more reliable method than extra-modification for enhanced the photocatalytic activity of ZrO_2.

8. Conclusion and prospects

ZrO_2 has been used as a photocatalyst in many chemical processes due to its comparatively wide E_g and the strong negative value of the CB potential. Nonetheless, intrinsic ZrO_2 with E_g of 5.0 eV is only responsive to UV light, making utilization of visible light impractical. Self-modification is an efficient approach to change its spectral response toward the visible light. Therefore, this review emphasizes a self-modification of ZrO_2 for enhanced the degradation of organic pollutants. The different preparation methods and alteration synthesis parameters are the approaches of self-modification of ZrO_2. These approaches can contribute to the difference of morphological, crystal structure, and surface defects of ZrO_2, which affected photoactivity. Various unique morphology of ZrO_2, including flower-like, nanowires, nanotubes, mesoporous and fibrous, represents the smallest dimension for efficient transport of e^- as well as an optical excitation. A higher crystallinity and phase stabilization of ZrO_2 material is supposed to be advantageous for photocatalysis. A defect site including OV-rich ZrO_2 inhibited the e^--h^+ recombination, resulting in high photoactivity for degrading organic pollutants under light irradiation since it can directly serve as adsorption sites. Although a particular concentration of Zr^{3+} could improve photocatalytic activity, it couldn't prevent photo-generated e^-–h^+ pairs from recombination quickly. The concentration of Zr^{3+} must be sufficient to create a continuous vacancy band of electronic states below the CB edge of Zr to achieve the efficient activity. As a result, a proper high concentration of defects is critical for improving photocatalytic efficiency. Hence, in order to generate defect sites, there are other techniques have been reported, which include heating under vacuum or high temperatures, irradiating with UV, reducing treatment, plasma-treating, etc.

Finally, all the above strategies by self-modification of ZrO_2 play critical roles in improving the catalytic performance. There are several modifications of ZrO_2 that have not yet been applied to enhance the photoactivity, including a combination of the Zr^{3+} self-doping with other traditional modifications such as metal and nonmetals doping. Moreover, it is recommended that the exploration of ZrO_2 photocatalyst in degrading other organic pollutants that are more harmful, including pesticides, pharmaceutical waste, antibiotics, and heavy metals, enhances the credibility of ZrO_2 in environmental remediation. In addition, little research has been published on the usage of ZrO_2 in a simultaneous reaction due to the presence of both heavy metals and organic contaminants in real wastewater. Then, the practical use of photocatalytic degradation of organic pollutants would also necessitate extensive research to scale-up laboratory investigations and enhance photoactivity, which is now poor. Last but not least, considering the vast potential of ZrO_2 in degrading the organic pollutants, it is a pleasure to explore this catalyst further for other applications such as photo-electrochemical water splitting, photoreduction of carbon dioxide into methanol, and gas-phase reaction. Overall, more attention should be directed towards the application of ZrO2 on real wastewater to achieve efficient pilot plant-scale production.

In the near future, it is hoped that an excellent ZrO_2 photocatalyst can be systematically fabricated for explicit photocatalytic applications with promising activity and selectivity. Additionally, it is envisaged that this review would aid in designing an efficient and reliable photocatalytic system.

CRediT authorship contribution statement

N.S. Hassan: Conceptualization, Investigation, Resources, Formal analysis, Visualization, Writing – original draft. **A.A. Jalil:** Writing – review & editing, Supervision, Project administration, Funding acquisition, Validation.

Declaration of Competing Interest

The authors declare that they have no known competing financial interests or personal relationships that could have appeared to influence the work reported in this paper.

Acknowledgment

The authors gratefully acknowledge the Universiti Teknologi Malaysia for the High Impact Research Grant (Grant No. 08G92) and Professional Development Research University Grant (No. 05E44).

Conflict of interest

The authors stated that there are no known conflicts of interest in this article.

References

Aminipoya, H., Ghomi, A.B., Rayati, S., 2020. ZrO_2 nanoparticles: optical properties of tetragonal phase and enhanced photocatalytic activity. J. Optoelectron. Nanostruct. 5, 2.

Azami, M.S., Jalil, A.A., Hitam, C.N.C., Hassan, N.S., Mamat, C.R., Adnan, R.H., Chanlek, N., 2020. Tuning of the electronic band structure of fibrous silica titania with g-C_3N_4 for efficient Z-scheme photocatalytic activity. Appl. Surf. Sci. 512, 145744.

Azami, M.S., Jalil, A.A., Hassan, N.S., Hussain, I., Fauzi, A.A., Aziz, M.A.A., 2021. Green carbonaceous material-fibrous silica-titania composite photocatalysts for enhanced degradation of toxic 2-chlorophenol. J. Hazard. Mater. 414, 125524.

Aziz, F.F.A., Jalil, A.A., Hassan, N.S., Hitam, C.N.C., Rahman, A.F.A., Fauzi, A.A., 2021. Enhanced visible-light driven multi-photoredox Cr (VI) and p-cresol by Si and Zr interplay in fibrous silica-zirconia. J. Hazard. Mater. 401, 123277.

Basahel, S.N., Ali, T.T., Mokhtar, M., Narasimharao, K., 2015. Influence of crystal structure of nanosized ZrO_2 on photocatalytic degradation of methyl orange. Nanoscale Res. Lett. 10, 73–80.

Cao, H.Q., Qiu, X.Q., Luo, B., 2004. Synthesis and room temperature ultraviolet photoluminescence properties of zirconia nanowires. Adv. Funct. Mater. 14 (3), 243–246.

Carević, M.V., Abazović, N.D., Novaković, T.B., Pavlović, V., Čomor, M.I., 2016. Zirconium dioxide nanopowders with incorporated Si^{4+} ions as efficient photocatalyst for degradation of trichlorophenol using simulated solar light. Appl. Catal. B 195, 112–120.

Deshmane, V.G., Adewuyi, Y.G., 2012. Synthesis of thermally stable, high surface area, nanocrystalline mesoporous tetragonal zirconium dioxide (ZrO_2): effects of different process parameters. Microporus Mesoporus Mat. 148 (1), 88–100.

Dhiman, P., Naushad, M., Batoo, K.M., Kumar, A., Sharma, G., Ghfar, A.A., Gagan Kumar, G., Singh, M., 2017. Nano $Fe_xZn_{1-x}O$ as a tuneable and efficient photocatalyst for solar powered degradation of bisphenol A from aqueous environment. J. Clean. Prod. 165, 1542–1556.

Dutta, A., Banerjee, P., Sarkar, D., Bhattacharjee, S., Chakrabarti, S., 2015. Degradation of trypan blue in wastewater by sunlight-assisted modified photo-fenton reaction. Desalin. Water Treat. 56, 1498–1506, 1498-150.

Dwivedi, R., Maurya, A., Verma, A., Prasad, R., Bartwal, K.S., 2011. Microwave assisted sol–gel synthesis of tetragonal zirconia nanoparticles. J. Alloy. Compd. 509 (24), 6848–6851.

Fagan, R., McCormack, D.E., Dionysiou, D.D., Pillai, S.C., 2016. A review of solar and visible light active TiO_2 photocatalysis for treating bacteria, cyaotoxins and contaminants of emerging concern. Mat. Sci. Semicond. Proc. 42, 2–14.

Fang, D., Luo, Z., Liu, S., Zeng, T., Liu, L., Xu, J., Xu, W., 2013. Photoluminescence properties and photocatalytic activities of zirconia nanotube arrays fabricated by anodization. Opt. Mater. 35 (7), 1461–1466.

Fang, W., Xing, M., Zhang, J., 2017. Modifications on reduced titanium dioxide photocatalysts: a review. J. Photochem. Photobiol. C 32, 21–39.

Fatah, N.A.A., Triwahyono, S., Jalil, A.A., Salamun, N., Mamat, C.R., Majid, Z.A., 2017. n-Heptane isomerization over molybdenum supported on bicontinuous concentric lamellar silica KCC-1: influence of phosphorus and optimization using response surface methodology (RSM). Chem. Eng. J. 314, 650–659.

Fauzi, A.A., Jalil, A.A., Mohamed, M., Triwahyono, S., Jusoh, N.W.C., Rahman, A.F.A., Tanaka, H., 2018. Altering fiber density of cockscomb-like fibrous silica–titania catalysts for enhanced photodegradation of ibuprofen. J. Environ. Manag. 227, 34–43.

Fauzi, A.A., Jalil, A.A., Hitam, C.N.C., Aziz, F.F.A., Chanlek, N., 2020. Superior sulfate radicals-induced visible-light-driven photodegradation of pharmaceuticals by appropriate Ce loading on fibrous silica ceria. J. Environ. Chem. Eng. 8 (6), 104484.
Gao, Q.X., Wang, X.F., Wu, X.C., Tao, Y.R., Zhu, J.J., 2011. Mesoporous zirconia nanobelts: preparation, characterization and applications in catalytical methane combustion. Microporous Mesoporous Mat. 143, 333–340.
Gionco, C., Paganini, M.C., Giamello, E., Burgess, R., Di Valentin, C., Pacchioni, G., 2013. Paramagnetic defects in polycrystalline zirconia: an EPR and DFT study. Chem. Mater. 25 (11), 2243–2253.
Gionco, C., Paganini, M.C., Chiesa, M., Maurelli, S., Livraghi, S., Giamello, E., 2015. Cerium doped zirconium dioxide as a potential new photocatalytic material. The role of the preparation method on the properties of the material. Appl. Catal. A 504, 338–343.
Gnanasekaran, L., Pachaiappan, R., Kumar, P.S., Hoang, T.K., Rajendran, S., Durgalakshmi, D., Gracia, F., 2021. Visible light driven exotic p (CuO)-n (TiO_2) heterojunction for the photodegradation of 4-chlorophenol and antibacterial activity. Environ. Pollut. 287, 117304.
Gorban, O., Synyakina, S., Volkova, G., Gorban, S., Konstantiova, T., Lyubchik, S., 2015. Formation of metastable tetragonal zirconia nanoparticles: competitive influence of the dopants and surface state. J. Solid. State Chem. 232, 249–255.
Guo, M.Y., Ng, A.M.C., Liu, F., Djurisic, A.B., Chan, W.K., Su, H., Wong, K.S., 2011. Effect of native defects on photocatalytic properties of ZnO. J. Phys. Chem. C. 115 (22), 11095–11101.
Haghjoo, H., Sangsefidi, F.S., Salavati-Niasari, M., 2017. Study on the optical, magnetic, and photocatalytic activities of the synthesized Mn_2O_3-SiO_2 nanocomposites by microwave method. J. Mol. Liq. 242, 779–788.
Hassan, N.S., Jalil, A.A., Triwahyono, S., Khusnun, N.F., Izan, S.M., Kidam, K., Johari, A., 2018a. Synergistic effect of microwave rapid heating and weak mineralizer on silica-stabilized tetragonal zirconia nanoparticles for enhanced photoactivity of Bisphenol A. J. Mol. Liq. 261, 423–430.
Hassan, N.S., Jalil, A.A., Triwahyono, S., Hitam, C.N.C., Rahman, A.F.A., Khusnun, N.F., Prasetyoko, D., 2018b. Exploiting copper–silica–zirconia cooperative interactions for the stabilization of tetragonal zirconia catalysts and enhancement of the visible-light photodegradation of bisphenol A. J. Taiwan Inst. Chem. Eng. 82, 322–330.
Hassan, N.S., Jalil, A.A., Khusnun, N.F., Ali, M.W., Haron, S., 2019. Role of reduced graphene oxide in improving interfacial charge transfer of hybridized rGO/silica/zirconia for enhanced Bisphenol A photodegradation. J. Alloy. Compd. 789, 221–230.
Hassan, N.S., Jalil, A.A., Aziz, F.F.A., Fauzi, A.A., Azami, M.S., Jusoh, N.W.C., 2020. Tailoring the silica amount in stabilizing the tetragonal phase of zirconia for enhanced photodegradation of 2-chlorophenol. Top. Catal. 63, 1145–1156.
Hassan, N.S., Jalil, A.A., Hussain, I., Fauzi, A.A., Azami, M.S., Saravanan, R., Hairom, N. H.H., 2021a. Intensification of toxic chlorophenolic compounds degradation over efficient microwave-dried silica-doped tetragonal zirconia nanocatalysts. Chem. Eng. Process. Process Intensif. 165, 108469.
Hassan, N.S., Jalil, A.A., Aziz, F.F.A., Aziz, M.A.H., Hussain, I., Ali, M.W., 2021b. New insight into sequential of silica-zirconia precursors in stabilizing silica-doped tetragonal zirconia nanoparticles for enhanced photoactivity. Mater. Lett. 291, 129582.
Hitam, C.N.C., Jalil, A.A., Triwahyono, S., Rahman, A.F.A., Hassan, N.S., Khusnun, N.F., Ahmad, A., 2018. Effect of carbon-interaction on structure-photoactivity of Cu doped amorphous TiO_2 catalysts for visible-light-oriented oxidative desulphurization of dibenzothiophene. Fuel 216, 407–417.
Ismail, S., Ahmad, Z.A., Berenov, A., Lockman, Z., 2011. Effect of applied voltage and fluoride ion content on the formation of zirconia nanotube arrays by anodic oxidation of zirconium. Corros. Sci. 53 (4), 1156–1164.
Jaafar, N.F., Jalil, A.A., Triwahyono, S., Shamsuddin, N., 2015. New insights into self-modification of mesoporous titania nanoparticles for enhanced photoactivity: effect of microwave power density on formation of oxygen vacancies and Ti^{3+} defects. RSC Adv. 5, 90991–91000.
Jaenicke, S., Chuah, G., Raju, V., Nie, Y., 2008. Structural and morphological control in the preparation of high surface area zirconia. Catal. Surv. Asia 12, 153–169.
Jalil, A.A., Triwahyono, S., Sapawe, N., Ahmed, I.H., Aziz, M.A.A., 2015. Low-temperature stabilization of electrosynthesized tetragonal zirconia, its photoactivity toward methylene blue decolorization. Desalin. Water Treat. 56 (9), 2402–2416.
Jiang, W., He, J., Zhong, J., Lu, J., Yuan, S., Liang, B., 2014. Preparation and photocatalytic performance of ZrO_2 nanotubes fabricated with anodization process. Appl. Surf. Sci. 307, 407–413.
Khan, S.A., Fu, Z., Wang, W., Wang, H., Asif, M., 2014. Hierarchical m-ZrO_2 nanorods template-free synthesis by hydrothermal method. Int. J. Appl. Ceram. Technol. 11 (3), 590–593.
Khataee, A., Gholami, P., Kayan, B., Kalderis, D., Dinpazhoh, L., Akay, S., 2018. Synthesis of ZrO_2 nanoparticles on pumice and tuff for sonocatalytic degradation of rifampin. Ultrason. Sonochem. 48, 349–361.
Kumar, S., Ojha, A.K., 2015. Oxygen vacancy induced photoluminescence properties and enhanced photocatalytic activity of ferromagnetic ZrO_2 nanostructures on methylene blue dye under ultra-violet radiation. J. Alloy. Compd. 644, 654–662.
Li, G., Guo, C., Yan, M., Liu, S., 2016. Cs_xWO_3 nanorods: realization of full-spectrum-responsive photocatalytic activities from UV, visible to near-infrared region. Appl. Catal. B 183, 142–148.
Lin, Z., Li, L., Yu, L., Li, W., Yang, G., 2017. Modifying photocatalysts for solar hydrogen evolution based on the electron behavior. J. Mater. Chem. A 5 (11), 5235–5259.
Liu, Y., Wang, J., Yang, P., Matras-Postolek, K., 2015. Self-modification of TiO_2 one-dimensional nano-materials by Ti^{3+} and oxygen vacancy using Ti_2O_3 as precursor. RSC Adv. 5 (76), 61657–61663.
López, U., Lemus, A., Hidalgo, M.C., López González, R., Quintana Owen, P., Oros-Ruiz, S., Acosta, J., 2019. Synthesis and characterization of ZnO-ZrO_2 nanocomposites for photocatalytic degradation and mineralization of phenol. J. Nanomater.
Lutterbeck, C.A., Wilde, M.L., Baginska, E., Leder, C., Machado, Ê.L., Kümmerer, K., 2015. Degradation of 5-FU by means of advanced (photo) oxidation processes: UV/H_2O_2, UV/Fe^{2+}/H_2O_2 and UV/TiO_2- comparison of transformation products, ready biodegradability and toxicity. Sci. Total. Environ. 527, 232–245.
Maheswari, A.U., Kumar, S.S., Sivakumar, M., 2013. Influence of alkaline mineralizer on structural and optical properties of ZrO2 nanoparticles. J. Nanosci. Nanotechnol. 13, 4409–4414.
Maheswari, A.U., Mohan, S.R., Kumar, S.S., Sivakumar, M., 2014. Phase tuning of zirconia nanocrystals by varying the surfactant and alkaline mineralizer. Ceram. Int. 40 (5), 6561–6568.
Mahmood, Q., Afzal, A., Siddiqi, H.M., Habib, A., 2013. Sol–gel synthesis of tetragonal ZrO_2 nanoparticles stabilized by crystallite size and oxygen vacancies. J. Sol. Gel Sci. Technol. 67 (3), 670–674.
Mahy, J.G., Lambert, S.D., Tilkin, R.G., Wolfs, C., Poelman, D., Devred, F., Douven, S., 2019. Ambient temperature ZrO_2-doped TiO_2 crystalline photocatalysts: highly efficient powders and films for water depollution. Mater. Today Energy 13, 312–322.
Majedi, A., Davar, F., Abbasi, A., Ashrafi, A., 2016. Modified sol–gel based nanostructured zirconia thin film: preparation, characterization, photocatalyst and corrosion behavior. J. Inorg. Organomet Polym. Mater. 26 (5), 932–942.
Melchor-Lagar, V., Ramos-Ramírez, E., Morales-Pérez, A.A., Rangel-Vázquez, I., Del Angel, G., 2020. Photocatalytic removal of 4-chlorophenol present in water using ZrO_2/LDH under UV light source. J. Photochem. Photobiol. A Chem. 389, 112251.
Moafi, H.F., Shojaie, A.F., Zanjanchi, M.A., 2010. The comparison of photocatalytic activity of synthesized TiO_2 and ZrO_2 nanosize onto wool fibers. Appl. Surf. Sci. 256 (13), 4310–4316.
Mustapha, F.H., Jalil, A.A., Mohamed, M., Triwahyono, S., Hassan, N.S., Khusnun, N.F., Zolkifli, A.S., 2017. New insight into self-modified surfaces with defect-rich rutile TiO_2 as a visible-light-driven photocatalyst. J. Clean. Prod. 168, 1150–1162.
Nagaveni, K., Sivalingam, G., Hegde, M.S., Madras, G., 2004. Solar photocatalytic degradation of dyes: high activity of combustion synthesized nano TiO_2. Appl. Catal. B 48 (2), 83–93.
Nasir, J.A., ur Rehman, Z., Shah, S.N.A., Khan, A., Butler, I.S., Catlow, C.R.A., 2020. Recent developments and perspectives in CdS-based photocatalysts for water splitting. J. Mater. Chem. A 8 (40), 20752–20780.
Nawale, A.B., Kanhe, N.S., Bhoraskar, S.V., Mathe, V.L., Das, A.K., 2012. Influence of crystalline phase and defects in the ZrO_2 nanoparticles synthesized by thermal plasma route on its photocatalytic properties. Mater. Res. Bull. 47 (11), 3432–3439.
Niu, P., Yin, L.C., Yang, Y.Q., Liu, G., Cheng, H.M., 2014. Increasing the visible light absorption of graphitic carbon nitride (Melon) photocatalysts by homogeneous self-modification with nitrogen vacancies. Adv. Mater. 26 (47), 8046–8052.
Oturan, M.A., Aaron, J.J., 2014. Advance oxidation processes in water/wastewater treatment: principles and applications. a review. Crit. Rev. Environ. Sci. Tec. 44, 2577–2641.
Pourakbar, M., Moussavi, G., Shekoohiyan, S., 2016. Homogenous VUV advanced oxidation process for enhanced degradation and mineralization of antibiotics in contaminated water. Ecotoxicol. Environ. Saf. 125, 72–77.
Rahman, A.F.A., Jalil, A.A., Triwahyono, S., Ripin, A., Aziz, F.F.A., Fatah, N.A.A., Hassan, N.S., 2017. Strategies for introducing titania onto mesostructured silica nanoparticles targeting enhanced photocatalytic activity of visible-light-responsive Ti-MSN catalysts. J. Clean. Prod. 143, 948–959.
Rajendran, S., Pachaiappan, R., Hoang, T.K., Karthikeyan, S., Gnanasekaran, L., Vadivel, S., Gracia-Pinilla, M.A., 2021. CuO-ZnO-PANI a lethal P-N-P combination in degradation of 4-chlorophenol under visible light. J. Hazard. Mater. 416, 125989.
Rashad, M.M., Baioumy, H.M., 2008. Effect of thermal treatment on the crystal structure and morphology of zirconia nanopowders produced by three different routes. J. Mater. Process. Technol. 195 (1–3), 178–185.
Reddy, C.V., Babu, B., Reddy, I.N., Shim, J., 2018. Synthesis and characterization of pure tetragonal ZrO_2 nanoparticles with enhanced photocatalytic activity. Ceram. Int. 44 (6), 6940–6948.
Rezaei, M., Alavi, S.M., Sahebdelfar, S., Yan, Z.F., 2006. Tetragonal nanocrystalline zirconia powder with high surface area and mesoporous structure. Powder Technol. 168, 59–63.
Rezaei, M., Alavi, S.M., Sahebdelfar, S., Xinmei, L., Yan, Z.F., 2007. Synthesis of mesoporous nanocrystalline zirconia with tetragonal crystallite phase by using ethylene diamine as precipitation agent. J. Mater. Sci. 42 (17), 7086–7092.
Rodriguez-Chueca, J., Amor, C., Fernandes, J.R., Tavares, P.T., Lucas, M.S., 2016. Treatment of crystallized-fruit wastewater by UV-A LED photofenton and coagulation-flocculation. Chemosphere 145, 351–359.
Santos, V., Zeni, M., Bergmann, C.P., Hohemberger, J.M., 2008. Correlation between thermal treatment and tetragonal/monoclinic nanostructured zirconia powder obtained by sol–gel process. Rev. Adv. Mater. Sci. 17 (1/2), 62–70.
Sapawe, N., Jalil, A.A., Triwahyono, S., Adam, S.H., Jaafar, N.F., Satar, M.A.H., 2012. Isomorphous substitution of Zr in the framework of aluminosilicate HY by an electrochemical method: Evaluation by methylene blue decolorization. Appl. Catal. B 125, 311–323.
Saravanan, R., Karthikeyan, N., Gupta, V.K., Thirumal, E., Thangadurai, P., Narayanan, V., Stephen, A., 2013. ZnO/Ag nanocomposite: an efficient catalyst for degradation studies of textile effluents under visible light. Mater. Sci. Eng. C 33, 2235–2244.
Sathishkumar, P., Mangalaraja, R.V., Anandan, S., 2015. Sonophotocatalytic mineralization of environmental contaminants present in aqueous solutions. Handb. Ultrason. Sonochem. 1–38.

Sato, S., Kadowaki, T., 1987. Photocatalytic activities of metal oxide semiconductors for oxygen isotope exchange and oxidation reactions. J. Catal. 106 (1), 295–300.
Shinde, H.M., Bhosale, T.T., Gavade, N.L., Babar, S.B., Kamble, R.J., Shirke, B.S., Garadkar, K.M., 2018. Biosynthesis of ZrO_2 nanoparticles from Ficus benghalensis leaf extract for photocatalytic activity. J. Mater. Sci. Mater. Electron. 29 (16), 14055–14064.
Shu, Z., Jiao, X., Chen, D., 2012. Synthesis and photocatalytic properties of flower-like zirconia nanostructures. CrystEngComm 14 (3), 1122–1127.
Shu, Z., Jiao, X., Chen, D., 2013. Hydrothermal synthesis and selective photocatalytic properties of tetragonal star-like ZrO_2 nanostructures. CrystEngComm 15 (21), 4288–4294.
Singh, B.R., Shoeb, M., Khan, W., Naqvi, A.H., 2014. Synthesis of graphene/zirconium oxide nanocomposite photocatalyst for the removal of rhodamineB dye from aqueous environment. J. Alloy. Compd. 651, 598–607.
Sinhamahapatra, A., Jeon, J.-P., Kang, J., Han, B., Yu, J.-S., 2016. Oxygen-deficient zirconia (ZrO2-x): a new material for solar light absorption. Sci. Rep. 6, 27218.
Siwińska-Ciesielczyk, K., Świgoń, D., Rychtowski, P., Moszyński, D., Zgoła-Grześkowiak, A., Jesionowski, T., 2020. The performance of multicomponent oxide systems based on TiO_2, ZrO_2 and SiO_2 in the photocatalytic degradation of Rhodamine B: mechanism and kinetic studies. Colloids Surf. A: Physicochem. Eng. Asp. 586, 124272.
Sreethawong, T., Ngamsinlapasathian, S., Yoshikawa, S., 2013. Synthesis of crystalline mesoporous-assembled ZrO_2 nanoparticles via a facile surfactant-aided sol–gel process and their photocatalytic dye degradation activity. Chem. Eng. J. 228, 256–262.
Stojadinović, S., Vasilić, R., Radić, N., Grbić, B., 2015. Zirconia films formed by plasma electrolytic oxidation: photoluminescent and photocatalytic properties. Opt. Mater. 40, 20–25.
Sultana, S., Khan, M.Z., Shahadat, M., 2015. Development of ZnO and ZrO_2 nanoparticles: their photocatalytic and bactericidal activity. J. Environ. Chem. Eng. 3 (2), 886–891.
Suresh, P., Vijaya, J.J., Kennedy, L.J., 2014. Photocatalytic degradation of textile-dyeing wastewater by using a microwave combustion-synthesized zirconium oxide supported activated carbon. Mater. Sci. Semicond. Process. 27, 482–493.
Suresh, R., Rajendran, S., Kumar, P.S., Vo, D.V.N., Cornejo-Ponce, L., 2021. Recent advancements of spinel ferrite based binary nanocomposite photocatalysts in wastewater treatment. Chemosphere 274, 129734.
Taguchi, M., Nakane, T., Matsushita, A., Sakka, Y., Uchikoshi, T., Funazukuri, T., Naka, T., 2014. One-pot synthesis of monoclinic ZrO_2 nanocrystals under subcritical hydrothermal conditions. J. Supercrit. Fluid. 85, 57–61.
Tao, X.Y., Ma, J., Hou, R.L., Song, X.Z., Guo, L., Zhou, S.X., Zhu, Y.B., 2018. Template-free synthesis of star-like ZrO_2 nanostructures and their application in photocatalysis. Adv. Mater. Sci. Eng. 2018, 1–10.
Teeparthi, S.R., Awin, E.W., Kumar, R., 2018. Dominating role of crystal structure over defect chemistry in black and white zirconia on visible light photocatalytic activity. Sci. Rep. 8 (1), 1–11.
Tsai, D.S., Chou, C.C., 2018. Review of the soft sparking issues in plasma electrolytic oxidation. Metals 8 (2), 105.
Ward, D.A., Ko, E.I., 1993. Synthesis and structural transformation of zirconia aerogels. Chem. Mater. 5 (7), 956–969.
Wierzbicka, E., Syrek, K., Mączka, K., Sulka, G.D., 2021. Photocatalytic decolorization of methyl red on nanoporous anodic ZrO_2 of different crystal structures. Crystals 11 (2), 215.
Wu, T., Shao, Q., Ge, S., Zhao, W., Liu, Q., 2016. Influence of molecular weight of chitosan on the microstructures and photocatalytic property of ZrO_2 prepared by chitosan templates method. Mater. Res. Bull. 83, 657–663.
Xavier, S., Gandhimathi, Nidheesh, P.V., Ramesh, S.T., 2015. Comparison of homogenous and heterogeneous fenton processes for the removal of reactive dye magenta MB from aqueous solution. Desalin. Water Treat. 53, 109–118.
Xie, C., Yan, D., Li, H., Du, S., Chen, W., Wang, Y., Wang, S., 2020. Defect chemistry in heterogeneous catalysis: recognition, understanding, and utilization. ACS Catal. 10 (19), 11082–11098.
Yaghmaeian, K., Moussavi, G., Alahabadi, A., 2014. Removal of amoxicillin from contaminated water using NH_4Cl-activated carbon: continuous flow fixed-bed adsorption and catalytic ozonation regeneration. Chem. Eng. J. 236, 538–544.
Zhang, J., Gao, Y., Jia, X., Wang, J., Chen, Z., Xu, Y., 2018. Oxygen vacancy-rich mesoporous ZrO_2 with remarkably enhanced visible-light photocatalytic performance. Sol. Energy Mater. Sol. Cells 182, 113–120.
Zhang, L., Wang, W., Sun, S., Sun, Y., Gao, E., Zhang, Z., 2014. Elimination of BPA endocrine disruptor by magnetic BiOBr@ SiO_2@ Fe_3O_4 photocatalyst. Appl. Catal. B 148, 164–169.
Zhao, J., Wang, X., Zhang, L., Hou, X., Li, Y., Tang, C., 2011. Degradation of methyl orange through synergistic effect of zirconia nanotubes and ultrasonic wave. J. Hazard. Mater. 188 (1–3), 231–234.
Zheng, H., Liu, K., Cao, H., Zhang, X., 2009. L-Lysine-assisted synthesis of ZrO_2 nanocrystals and their application in photocatalysis. J. Phys. Chem. C 113 (42), 18259–18263.
Zinatloo-Ajabshir, S., Salavati-Niasari, M., 2016. Facile route to synthesize zirconium dioxide (ZrO_2) nanostructures: structural, optical and photocatalytic studies. J. Mol. Liq. 216, 545–551.